PHILOSOPHICAL TRANSACTIONS OF THE ROYAL SOCIETY A MATHEMATICAL, PHYSICAL & ENGINEERING SCIENCES

Vortical Structures and Coherent Motion in Turbulent Flow over Smooth and Rough Boundaries

A. J. Grass, R. J. Stuart and M. Mansour-Tehrani

Phil. Trans. R. Soc. Lond. A 1991 **336**, 35-65
doi: 10.1098/rsta.1991.0065

Vortical structures and coherent motion in turbulent flow over smooth and rough boundaries

By A. J. Grass, R. J. Stuart and M. Mansour-Tehrani

Department of Civil and Environmental Engineering, University College London, Gower Street, London WC1E 6BT, U.K.

It has been recognized for some years that the bursting phenomenon is a common feature of turbulent boundary layers irrespective of wall roughness condition. In confirmation of Theodorsen's original conjecture, there is now a convincing body of evidence, particularly deriving from recent direct numerical simulation studies, that the dynamics of this bursting process over smooth walls, is directly linked to the presence of powerful vortical structures with a general horseshoe-type configuration, embedded in the wall flow field. The present paper describes the results of physical experiments which demonstrate that these vortex structures are also present in turbulent boundary layers over rough walls and that they are similarly linked to the bursting events. Novel velocity measurement techniques were used in the investigation which, for the first time in physical fluid mechanics research, allowed quasi-instantaneous vortex lines to be traced through a three-dimensional block of flow space to reveal the vortical structures. The preliminary results from a second investigation are also presented which demonstrate that, just as in the smooth wall case, the spanwise flow structure adjacent to a rough boundary exhibits a well defined cross-flow wavelength. The measurements indicate that this wavelength, which reflects the spanwise scale of the near-wall vortex structures, is directly proportional to the size of the boundary roughness elements under fully rough conditions. Consistent with Townsend's 'attached-eddy' hypothesis, the vortical structures are observed to increase in scale with increasing wall distance while remaining attached back to the vorticity generation zone at the boundary. The paper commences with a review of the status of current knowledge relating to coherent vortical structures in turbulent boundary layers and its interpretation in the context of large scale geophysical flows.

1. Introduction

It is interesting to speculate on what a very different world we would inhabit if there was no such thing as a critical Reynolds number and water and air flows over the surface of the globe remained in a laminar rather than their normal turbulent state. In the absence of man-made controls, a modest scale river such as the Thames, with a depth of several metres and a 'walking pace' current velocity, would be transformed into a shallow, swiftly moving sheet flow, a fraction of a metre deep and with surface velocity commensurate with that of a motor car. To restore the turbulent depth and low mean velocity, the fluid viscosity in a corresponding laminar flow would need to be increased by three orders of magnitude. Under laminar flow

Phil. Trans. R. Soc. Lond. A (1991) **336**, 35–65
Printed in the U.K.

2-2

conditions the largest rivers, such as the Amazon, would assume spectacular surface velocities of several hundred kilometres per hour.

Paradoxically, therefore, turbulence actually promotes tranquility in our everyday surroundings by greatly slowing down current velocities in rivers and streams through the action of very large effective eddy viscosities. Also, contrary to intuitive expectations, since the bed shear stress in uniform, free surface water flow is proportional to the depth, high-speed laminar rivers would exert far smaller forces on the boundary than their turbulent counterparts. Sediment transport would therefore be drastically reduced, particularly in the absence of a suspension transport mode which requires boundary-layer turbulence. The geomorphology and topographical character of the eroded landscape would thus be radically altered.

These profound and dramatic changes serve to emphasize the crucial role played by turbulence in shaping our real natural environment. With the ever increasing concern over and awareness of the gravely deleterious impact of man's violent abuse of the environment over the past two centuries, turbulence, as a major transporting and diffusing agent for pollutants, heat, and other passive and non-passive contaminants, assumes new levels of importance. There is, for example, an urgent need to improve the effectiveness of boundary-layer turbulence models for predicting the behaviour of surface water and atmospheric flow systems. Such information represents an essential input for environmental impact assessment in addition to the traditional requirements of engineering design. Effective model development in turn demands substantial improvements in our understanding and knowledge of the mechanics of turbulence, particularly in large-scale, geophysical boundary layers.

In a survey lecture to the Osborne Reynolds Centenary Symposium, Lighthill (1968) observed that following the major initial contributions to the science of turbulence by Reynolds, subsequent progress has been slow and a clear reflection of the formidable complexities of the phenomenon. Lighthill also drew attention to the fact that advances in knowledge, when they have occurred, have invariably been linked to the introduction of either new experimental or theoretical techniques. Reynolds himself, for example, used dye injection to reveal the clear distinction between laminar and turbulent flow, and the onset of instability and transition in pipe flow. Consistent with this trend, in more recent times, Kline *et al.* (1967) also made imaginative use of a relatively simple but novel flow visualization method, namely the hydrogen bubble flow tracer technique, to identify and investigate the 'bursting' phenomenon in turbulent boundary layers.

Kline and his co-workers gave a detailed description of the streaky nature of the flow structure in the viscous sublayer on a smooth wall with its alternating narrow, elongated zones of high and low fluid velocity. They linked this streaky structure to the bursting process which they described as a randomly occurring event comprising gradual local lift-up of the fluid in the low-speed streaks, sudden oscillation, bursting and ejection. This bursting and ejection phenomenon is closely associated with sweep and energetic inrush events, identified and described respectively by Corino & Brodkey (1969) and by Grass (1971), based on observations from similar visualization studies of the boundary-layer flow structure. The inrush events bring high-speed fluid in close to the boundary, forming the high-speed streaks. This action intensifies near-wall vorticity by lateral spanwise stretching, and also generates new vorticity which is subsequently transported away from the wall by the ejections.

The ejection and inrush events form linked parts of a random, cyclical process of

PHILOSOPHICAL TRANSACTIONS OF THE ROYAL SOCIETY A MATHEMATICAL, PHYSICAL & ENGINEERING SCIENCES

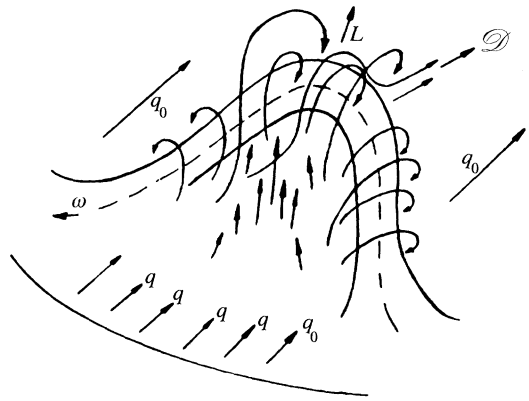

Figure 1. Horseshoe vortex model first proposed by Theodorsen (1952).

turbulence generation in the boundary layer involving recurring instability. This process has been shown to be responsible for most of the turbulence energy production and the major contribution to the Reynolds stress momentum transport in the wall layers. The necessary existence of such a pattern of inward and outward transport of fluid was deduced by Lighthill (1963). His simple but convincing argument is that it probably represents the only means by which the very large gradients in mean vorticity present at the wall in turbulent boundary layers, can be maintained against the correspondingly large outward diffusion and transport of vorticity by viscous and ejective turbulence action. It is important to note that this argument applies independently of wall roughness. One can therefore expect similar patterns of fluid motion over rough boundaries. Grass (1971, 1982) confirmed this expectation and clearly demonstrated the existence of both violent ejection and inrush events over rough walls. It was concluded that these were common features of boundary-layer turbulence irrespective of wall roughness condition.

The common presence of these dominant inrush and ejection structural features, suggests that a shared mechanism could be responsible for their generation. Based on a combination of rational analysis and remarkable intuitive physical insight, Theodorsen (1952) proposed a simple vortex model as the central element of the turbulence generation process in shear flows. This took the form of a horseshoe-shaped vortical structure inclined in the direction of mean shear illustrated in the author's original diagram reproduced in figure 1. Theodorsen conjectured, with extraordinary foresight in the light of evidence now emerging, that this vortex structure is a common feature of all shear layers being present not only in wall-bounded flows but also in free shear layers, laminar to turbulent transition and even sheared homogeneous turbulence.

Since Theodorsen's paper was published almost four decades ago, a plethora of turbulence structure models has been proposed by numerous investigators. These typically involve similar single or multiple configurations of horseshoe-shaped (frequently referred to as 'hairpin') vortical structures. Comprehensive reviews of these conceptual models have been given by Wallace (1985) and more recently by Robinson (1989). Many of these models have been constructed, often with considerable ingenuity, on the basis of either consistency with velocity or pressure correlation measurements, or inferred from a wide variety of flow visualization studies, almost invariably yielding incomplete images. Probably the most complete

and convincing evidence of the existence of vortical structures embedded in fully developed turbulent boundary layers has come from recent computational studies. The successful development of effective 'direct' and 'large eddy' numerical simulations of turbulent flows over the past decade, resulting from the availability of sufficiently powerful digital computers, represents another fine example of the impact of new techniques in promoting advances in turbulence science.

Using data generated by numerical simulations of channel flow, Moin & Kim (1982, 1985) and Kim & Moin (1986) were able to identify horseshoe-type vortical structures clearly throughout the wall boundary layer. As might be expected, given the highly irregular three-dimensional distribution of background vorticity and fluid motion, and the similarly contorted form of internal shear layers in a turbulent boundary layer, these vortex loops appear as considerably distorted and frequently asymmetrical versions of the symmetrical horseshoe configuration shown in Theodorsen's idealized illustration (figure 1).

Kim & Moin also firmly established a strong link between these structures and ejection and sweep and inrush events from both instantaneous realizations and ensemble averages. Consistent with Theodorsen's description, upward looping vortices of the form shown in figure 1, with their self-induced velocity away from the wall and strong updraught currents between the side limbs (figure 1), were found to be associated with ejection events. Sweep and inrush events were similarly linked to the presence of inverted, downward-pointing horseshoes. Both types of structure are therefore associated with large contributions to Reynolds shear stress and turbulence production.

Guezennec *et al.* (1989) used a conditional averaging scheme, which preserved any lack of symmetry in Reynolds stress-producing events, to analyse data obtained in a direct numerical simulation of a low Reynolds number channel flow. It was concluded on the basis of their findings that these ejection and inrush and sweep events were predominantly associated with the presence of apparently asymmetrical vortical structures in the wall layer. A typically distorted and asymmetrical horseshoe vortex with limb positions staggered in the streamwise direction, or indeed with one of the limbs missing due to lack of roll-up in a relatively weak shear layer, is entirely consistent with this observed asymmetry in the velocity vector representations of the averaged and instantaneous structure. This conclusion is also strongly supported by the simulation results presented by Lyons *et al.* (1989). Both these structural characteristics are evident in the examples of horseshoe-shaped vortical structures presented by Kim & Moin (1986). The formation of low-speed streaks and subsequent bursting and ejection have been shown to develop under the pressure field influence of a single side or limb of a horseshoe-type structure. This has been clearly demonstrated in the effectively combined flow visualization and theoretical modelling studies reported by Smith *et al.* (1989) and by Walker (1990). Thus, while the counter-rotating leg vortices of a symmetrical horseshoe configuration produce similar wall layer eruption and ejection events, such symmetry is not essential for the turbulence production process.

Though also emphasizing the typically irregular and fragmented form of the vortical elements and structures, Robinson (1989) largely confirms the above conclusions regarding their ubiquitous presence throughout the boundary layer and the basic horseshoe configuration to which they conform. Robinson *et al.* (1989) carried out an extensive analysis of the database generated in a numerical simulation of a flat plate boundary layer reported by Spalart (1988). Making creative use of

PHILOSOPHICAL TRANSACTIONS OF THE ROYAL SOCIETY A MATHEMATICAL, PHYSICAL & ENGINEERING SCIENCES

innovative, three-dimensional motion computer graphics, it was possible in this study to examine the time evolution of the vortical structures and hence to establish a more detailed picture of their direct links with ejection and sweep/inrush events.

Kline & Robinson (1989) presented a progress review of a current community-wide cooperative study of boundary layer structure which included an assessment and interpretation of recent numerical simulation studies. They draw the firm conclusion that powerful vortical structures, apparently representing rolled-up elements of typically incompletely developed horseshoe form, represent the central feature of the turbulence generation process. Robinson (1989) uses a very apt expression for the key role of these vortical structures, describing them as 'pumps'. The weight of existing evidence suggests that these vortical pumps are the primary agent for transport of mass, momentum, vorticity, heat and other contaminants, outwardly and inwardly across the boundary layer. They derive their energy from the mean flow by the simple mechanism of vortex stretching. Thus the essential demands regarding the basic inward and outward transport characteristics of the boundary layer flow field deduced by Lighthill (1963) and discussed previously, are satisfied. Vortical structures provide the necessary mechanism for maintenance of the high-vorticity layer at the wall against large outward vorticity transport, their other primary role.

The rapid advances in powerful computational research tools over the past decade has undoubtedly made a major and exciting new contribution to improved understanding of turbulence physics. The uniquely comprehensive pressure and velocity field information available from these techniques is particularly valuable in the development of more effective models for engineering calculation. All the indications are that the impact of numerical simulation will continue to grow in future years. Experience to date certainly confirms, as expected, that the Navier–Stokes equations represent an equally effective foundation model for calculating the complex detail of turbulent flow fields as for their laminar flow counterparts. However, fundamental limitations continue to be imposed by restricted computer capacity and its effect on choice of computation grid dimensions, and hence resolution of small-scale flow structure. There therefore remains an important need for high quality physical experiments to validate simulation results. Such testing will inevitably be required in the foreseeable future in investigations at high Reynolds numbers. Geophysical flows fall very much into this category and are likely to be well beyond the computational scope of direct numerical simulations for many years to come. Large-eddy simulation methods may help circumvent some of these problems for certain restricted tasks. Additional difficulties arise in the specification of computational boundary conditions for rough wall flows. This will undoubtedly again require long-term input of roughness data derived from physical experimental measurements.

In view of the vast body of research effort over the years, it is somewhat surprising that direct visual evidence of the existence of horseshoe-type vortical structures remains extremely restricted. This probably reflects a combination of the inherent difficulty of the task, lack of attention to development of specially designed visualization techniques and also the fragmented and incomplete form of the rolled-up vortex elements and structures reported by Kline & Robinson (1989) and Robinson (1989). Probably the most positive 'sightings' are recorded in the photographic images produced in the flow visualization studies of Head & Bandyopadhyay (1981). This study was particularly valuable as it covered a

PHILOSOPHICAL TRANSACTIONS OF THE ROYAL SOCIETY A MATHEMATICAL, PHYSICAL & ENGINEERING SCIENCES

relatively wide range of Reynolds numbers and identified important changes in the general flow structure as the ratio between boundary-layer thickness and the viscous wall length scale (Reynolds number) increased. Direct visual evidence of streamwise and transverse vortices in turbulent boundary layers, presumably forming restricted view elements of three-dimensional vortical structures, is extensively reported in the literature, for example, by Kim *et al.* (1971), Grass (1971) (1982), Clark & Markland (1971), Nychas *et al.* (1973), Praturi & Brodkey (1978), Smith & Schwartz (1983), Kasagi *et al.* (1986) and Smith & Lu (1988).

A considerable amount of indirectly supportive visual evidence does, however, exist, demonstrating the clear presence of three-dimensional vortex structures formed in wall shear layers during transition from laminar to turbulent flow, in tripped laminar boundary layers, and in turbulent spot development as presented, for example, by Hama & Nutant (1963), Williams *et al.* (1984), Acarlar & Smith (1987) and Perry *et al.* (1981). Further evidence of the formation of horseshoe vortices in shear flows in general, consistent with Theodorsen's conjecture, are given, for example, by Muller & Gyr (1986) in the separated mixing layer downstream of two-dimensional sand dunes, by Sene *et al.* (1989) in planar plunging jets, by Ferre *et al.* (1990) in the plane turbulent wake behind a circular cylinder, and perhaps most significantly, and again confirming Theodorsen's predictions, by Rogers & Moin (1987) and Lee *et al.* (1990) in sheared homogeneous turbulence.

The evidence for the existence of horseshoe/hairpin-type vortical structures in turbulent boundary layers outlined above and comprehensively reviewed with positive conclusion by Wallace (1985) and by Robinson (1989) is now very convincing. However, uncertainties remain concerning the mechanics of their formation and their dynamic role in the bursting process. Perhaps most conspicuously, there is a yawning gap of ignorance regarding the growth mechanism linking the small-scale, wall-layer horseshoe structures with the conjectured very large-scale structures present in the outer flow at extremely high Reynolds number. For example, in a hypothetical atmospheric boundary layer flow over a smooth surface, these scales might typically range between a few millimetres to several hundred metres, a ratio of the order 10^5.

Inspection of the vortex-stretching terms in the simple inviscid vorticity equations indicates that, when the initially parallel vortex lines in an idealized plane shear layer are subjected to a local velocity perturbation perpendicular to the plane, they deform into a natural horseshoe configuration. The horseshoe is inclined in the direction of shear and loops either upwards, in response to positive perturbation velocities such as occur during ejection events, or downwards for negative velocities produced by sweep and inrush events. Ensemble averages of the vortex lines associated with ejection and sweep events presented by Kim & Moin (1986) provide excellent confirmation of these predictions, forming symmetrical horseshoe configurations inclined upwards and downwards at approximately 45° to the channel walls in the outerflow region. This angle coincides with the principal axis along which the rate of strain and vortex stretching, and hence vorticity gain and energy absorption, are maximum. The hairpin vortices observed by Head & Bandyopadhyay (1981) also tended to be inclined at this characteristic 45° angle. These observations led Kim & Moin to conclude that the vortex stretching process, which also represents a central element in Theodorsen's analysis, is the proper mechanism for the formation of horseshoe vortices and a dominant flow mechanism.

The fact that horseshoe vortices were observed to form in the outer region of the

PHILOSOPHICAL TRANSACTIONS OF THE ROYAL SOCIETY A MATHEMATICAL, PHYSICAL & ENGINEERING SCIENCES

boundary layer remote from wall influence, prompted Kim & Moin to further conjecture, in line with Theodorsen's suggestion, that such structures are a universal feature of all shear flows, with or without a wall, the essential requirement for their formation being the presence of vortex stretching due to the strain field. Once again exploitation of recent developments and massive expansion in computational capacity has produced important new advances in knowledge by allowing these speculations to be tested. Rogers & Moin (1987) and Lee *et al.* (1990) have used direct numerical simulation techniques to explore the effects of applying shear to an initially homogeneous turbulence field. At moderate shear rates, horseshoe vortex structures were observed to form, apparently under the action of vorticity stretching along the direction of mean straining and initially inclined at an angle of 45° to the flow direction. At higher shear rates a distinct 'streaky' pattern appeared in the velocity field, closely similar to the elongated high- and low-velocity streaks formed in the strongly sheared viscous sublayer of wall-bounded flows. These remarkable findings directly confirm Theodorsen's inspired conjectures, and provide powerful new support for the concept of a dominant turbulence generation mechanism and structure common to all shear flows.

Lee *et al.* (1990) also applied rapid-distortion theory to calculate the sheared development of the instantaneous, initially homogeneous, flow field. The results showed very close similarity with the instantaneous velocity field patterns generated by direct numerical simulation of the full Navier–Stokes equations. The rapid-distortion approximation of the equations of motion which neglects nonlinear interaction between the turbulent fluctuations during distortion, is linear and provides a means of calculating changes to the turbulence structure and characteristics induced by variations in the mean velocity field produced by irrotational strain and shear. (See, for example, Townsend (1976), Hunt (1978) and Moffatt (1981) for review and discussion of the method.) Moffatt (1967) and Townsend (1970) were the first to apply this linearized approach to sheared flows. Townsend demonstrated the success of the method in obtaining excellent agreement between calculated and measured values of the velocity correlation functions for a turbulent wake flow. The scope of rapid-distortion analysis was very significantly extended by Hunt (1973) to take account of non-homogeneous distortions and the boundary conditions imposed on the turbulence by the presence of a wall. While, consistent with the underlying assumptions, this simplifying theory works best when flow distortions are indeed 'rapid', its predictive success for both statistical and instantaneous flow field characteristics strongly suggests that the dominant features of the physics of shear layer turbulence generation are captured. A key feature appears to be the selective amplification of turbulence structures involving processes which include the vortex stretching mechanism discussed previously.

There is also wide-ranging evidence from both flow visualization and numerical simulation studies (reviewed by Kline & Robinson (1989) and Robinson (1989)) that the phenomenon of free shear layer instability and roll-up, which concentrates vorticity into discrete vortex filaments, also plays a central role in the generation of horseshoe-type structures. As might be expected, internal shear layers embedded in turbulent boundary layers are highly irregular and three-dimensional. They are observed to form over the top and sides of low-speed wall streaks and ejected masses of outward-moving, low-velocity fluid, at the interface with the high-velocity surrounding fluid which is displaced and forced to flow over and round the obstruction. Because of the mean velocity gradient in the sheared flow, the largest

PHILOSOPHICAL TRANSACTIONS OF THE ROYAL SOCIETY A MATHEMATICAL, PHYSICAL & ENGINEERING SCIENCES

velocities are intercepted at the level of the top of the slow-moving fluid mass and form the most intense shear layers. These tend therefore to roll-up first, producing the 'head' elements of the horseshoe structures. The inclined vortex lines in the side shear layers are stretched, which intensifies the vorticity. This in turn accelerates the roll-up action to form the head connecting leg-elements of the horseshoe or part-horseshoe vortical structures, as observed and described by Kline & Robinson (1989). Blackwelder & Swearingen (1988) have drawn attention to the fact that the three-dimensional shape of the free-shear layers forming around low-speed wall streaks produces inflection points in both the normal and spanwise distributions of streamwise velocity. They suggest that in the context of the viscous wall-region flow, where the persistence time of the low-speed streaks is large compared with the instability time scale, inflectional instabilities could potentially develop in both the normal and spanwise shear layers. Consistent with this reasoning, instances of vortex roll-up occurring independently in the shear-layers along the sides of low-speed streaks have been reported by Kline & Robinson (1989).

Mean flow energy is fed into the vortex structures very rapidly during this formation process, involving the combined shear-layer roll-up and vorticity-stretching mechanism. This swift transfer of energy is certainly consistent with the relatively violent nature of the ejection and inrush events commented on, for example, by Grass (1971). A detailed and comprehensive picture of the feedback link between the vortical structures and the bursting process has still to emerge however. Plausible interpretations include a mechanism of direct induction on the wall layers during the passage of an overlying vortical structure favoured by Acarlar & Smith (1987) and Robinson *et al.* (1989) for example. Improved methods for calculation of flow separation in unsteady boundary layers, described for example by Cowley *et al.* (1990), Peridier *et al.* (1991 *a*, *b*), and Smith (1991), which again exploit computational advances, are now beginning to make a significant contribution to our understanding of the basic physics of the bursting process. It has been demonstrated using these techniques (see Walker & Herzog 1988) that the viscous–inviscid interaction induced by the pressure gradient generated by a moving vortex near the wall, can produce a violent eruption of the wall layer fluid. Smith & Walker (1990) and Walker (1990) suggest a direct link between these predicted eruptions and the bursting phenomenon and also the formation of new horseshoe structures. Evidence of such a self-induced process of structure regeneration has been provided by the flow visualization studies reported by Perry *et al.* (1981) and by Smith *et al.* (1989). The transverse propagation and spread of horseshoe structures also observed in these fundamental experiments has been reproduced in the theoretical computational studies of vortex filament distortion in a wall shear layer reported by Hon & Walker (1988). This provides another example of the increasingly important contribution of theoretical modelling to improved knowledge in this exceedingly complex area of mechanics.

The area of major weakness in our current understanding of boundary layer turbulence structure concerns the mechanics of structural growth. At the Reynolds numbers typically encountered in geophysical flows in rivers, tidal currents and the atmospheric boundary layer, for example, the ratio between the size of the largest eddies, which scale with the boundary layer thickness, and the typical dimension of the wall-layer structures, which relate to the viscous or wall roughness length scale, becomes extremely large, as mentioned previously. This has important, complicating, implications for the near-wall turbulence characteristics as illustrated by the following hypothetical situation.

PHILOSOPHICAL TRANSACTIONS OF THE ROYAL SOCIETY A MATHEMATICAL, PHYSICAL & ENGINEERING SCIENCES

Imagine an atmospheric boundary layer several hundred metres thick, developed over the aerodynamically smooth surface of a vast frozen lake. For a moderate mean wind speed of, say, 10–20 m s^{-1}, the streak spacing characterizing the dimension of the horseshoe-type vortical structures in the wall layer would be a few millimetres. Head & Bandyopadhyay's (1981) observations showed that very few of the wall-layer vortex structures survived in their extremely stretched state beyond a wall distance of say 50 wall streak spacings. In the situation under consideration, therefore, the small wall vortices would only be capable of outwardly diffusing vorticity throughout a thin 'carpet' layer, of order $\frac{1}{10}$ m thick, above the ice surface. The obvious question therefore arises as to how the flow lifts and distributes vorticity out to wall distances of several hundred metres.

Intuitively, the most physically plausible explanation is that there must be some form of continuous hierarchy of horseshoe structures with typical local size commensurate with, and increasing with, wall distance. The structure scale essentially determines the height to which it can 'pump' vorticity. Progressively larger vortical structures take over and continue this process up to the largest scales which relate to the local boundary layer thickness as conjectured by Theodorsen (1952). Such a continuous range of eddy scales is a central feature of Townsend's (1976) 'attached-eddy' hypothesis which Townsend represented in the simplified form of a double vortical cone structure in contact with, and hence attached to, the wall along its entire length. Perry & Chong (1982) and Perry *et al.* (1986, 1987) extended Townsend's hypothesis, proposing a more detailed eddy model, partly inspired by the flow visualization observations of Head & Bandyopadhyay (1981). In this model the turbulence structure is envisaged to consist of a hierarchical assemblage of grouped horseshoe-type vortices with average scale again increasing with wall distance. Common experience and observation provide convincing evidence of the presence of a wide range of structural scales in atmospheric boundary layer turbulence. For example, wind gusts with duration measured in tens of seconds indicate the presence of eddies with scale commensurate with the boundary layer thickness. Intermediate scale eddies are also frequently revealed in the relatively large streaky patterns visualized by powder snow or sand, blown across flat surfaces. Very clear evidence of intermediate scale eruptive, ejection structures is frequently observed in wind-blown dust plumes in the ground layers of atmospheric flow. The streamwise profile shape and violently eruptive character of these visualized atmospheric structures, are remarkably similar to the corresponding patterns and behaviour visualized in laboratory scale boundary layers (see, for example, Falco 1977; Head & Bandyopadhyay 1981; Gad-el-Hak *et al.* 1981; Grass 1982; Smith *et al.* 1991). This striking geometrical and dynamical correspondence across such a vast range of scales is certainly consistent with the concept of a scale hierarchy of geometrically similar, plume-generating eddies.

Returning to the hypothetical frozen lake situation, the wall-layer streak spacing will adjust to, and essentially follow, the low-frequency variations in background flow induced by the large-scale gusting structure. This is equivalent to very slowly increasing and then reducing the mean velocity in a wind tunnel boundary layer test. In these circumstances the near-wall turbulence characteristics and mean velocity profile continuously adjust to and scale with the prevailing quasi-steady flow conditions. Townsend (1961) and Bradshaw (1967) introduced the concept of 'active' and 'inactive' motion to explain the apparent Reynolds number dependency of certain correlation functions near the wall. The 'active' motion was linked to locally

PHILOSOPHICAL TRANSACTIONS OF THE ROYAL SOCIETY A MATHEMATICAL, PHYSICAL & ENGINEERING SCIENCES

scaled eddies which generate Reynolds shear stress, while the 'inactive' motion was deemed to be associated with very large-scale eddies which simply slowly accelerate and decelerate the wall flow and make little direct contribution to local Reynolds shear stress. The effect has profound implications for very high Reynolds number flows, since the law of the wall, based on the long-term averaged value of wall shear stress breaks down, as discussed in detail by Townsend (1976, ch. 5).

The mean velocity distribution is fortunately little affected by this breakdown except at very large geophysical scale Reynolds numbers when the amplitude of the low-frequency fluctuations in mean wall velocity about the long-term average becomes significant. However, very significant and systematic divergence occurs in the magnitude of the streamwise component of turbulence intensity, for example, with much larger values recorded in the atmospheric boundary layer than in laboratory scale tests (Townsend 1976). The Reynolds number influence is apparent even at modest laboratory scale Reynolds numbers, as evidenced by the carefully controlled spectral measurements presented by Perry *et al.* (1987) and corresponding results from numerical simulation by Spalart (1988). These findings have practical implications, for example, in the area of sediment transport. The transport of loose boundary sediment by either water or wind flows is strongly influenced by turbulence intensity (Grass 1982). The breakdown of wall similarity means that differences must be expected between laboratory-based observations and corresponding behaviour at geophysical scales.

The growth mechanism whereby the vortical structures expand in scale with increasing wall distance remains the subject of considerable speculation. Perry & Chong (1982), for example, suggest that vortex pairing, observed in free shear layers, jets and wakes, might conceivably play a part. Such pairing has been observed for artificially induced horseshoe vortices in laminar boundary layers and in computational model simulations reported by Smith *et al.* (1989). The process of merging and coalescence of low speed streaks in the viscous wall region of a turbulent boundary layer reported by Nakagawa & Nezu (1981) and by Smith & Metzler (1983) has been linked by these authors to the observed increase in streak spacing with wall distance. This increase may reflect scale growth in the associated horseshoe structures. Jimenez (1983) suggests cancellation of vorticity in adjacent 'leg' vortices with re-connection of the transverse 'head' vortices as a possible explanation of the observed growth in spanwise structure in a plane shear layer. Head & Bandyopadhyay (1981) proposed a similar growth process of vorticity cancellation with preservation of spanwise 'head' vorticity, for assemblages of hairpin vortices in turbulent boundary layers. In the imagined frozen lake flow, intuitive reasoning suggests that the thin carpet layer of relatively intense vorticity, discussed previously, might well be susceptible to the same regenerative mode of instability as the very thin, underlying, viscous sublayer. The resulting horseshoe-type vortical structure would then presumably scale on some effective eddy viscosity and averaged strain rate for the carpet layer. It can similarly be envisaged that this idealized process could be repeated across the entire boundary layer thickness with ever-increasing structure scale, to form the scale hierarchy suggested in the Townsend & Perry models.

The latter speculative observations appear to link in to the important findings reported by Rogers & Moin (1987) and Lee *et al.* (1990) in which horseshoe vortical structures were found to form in sheared homogeneous turbulence. There would appear to be no good reason, in principle, why the same selective amplification

PHILOSOPHICAL TRANSACTIONS OF THE ROYAL SOCIETY A MATHEMATICAL, PHYSICAL & ENGINEERING SCIENCES

mechanism responsible for organizing and concentrating vorticity in such an unordered flow field should not generate similar coherent structures from the random matrix of vortical structured elements and general vortical debris present, as demonstrated by the simulation results of Kline & Robinson (1989), in the near-wall layers under discussion. The vortex-stretching process then provides one possible growth mechanism for increasing the scale of these vortical structures, once formed. This growth will in turn reflect in the spectral wavelengths which ultimately determine the scale of further newly formed vortices downstream (Lee *et al.* 1990). Rogers & Moin (1987) also found that long spanwise vortices appeared in the simulated flow field at relatively late times in the flow development. It was speculated that these might represent connected tip elements of decayed horseshoe structures following the suggestions by Head & Bandyopadhyay (1981). Such spanwise vortices are of course inherently unstable as demonstrated, for example, by Hama (1962) and Hon & Walker (1988), and will ultimately deform into enlarged horseshoe vortices. It would certainly be interesting to run the numerical simulations of sheared homogeneous flow for longer shear times to seek evidence of progressive scale growth in the newly formed horseshoe vortices. Also relevant to this discussion of scale growth, is the fact that large horseshoe vortices have been observed to develop from roll-up of turbulent, free-shear layers as, for example, in the wake flow downstream of bluff cylinders and downstream facing bed steps (Muller & Gyr 1986). Karman vortex streets have also been commonly observed at very large geophysical scales, forming from roll-up of the extremely thick turbulent shear layers separating from islands in tidal streams and from isolated mountain peaks in atmospheric flows.

The above outline review has attempted to summarize the current status of knowledge regarding coherent vortical structures in turbulent boundary layers and their role in turbulence generation. It is clear from this discussion that an overwhelming majority of the investigations carried out to date relate to smooth wall flow. This is exclusively the case for the crucially important numerical simulation studies which can at present only cope with the simple smooth wall boundary condition. The investigations reported in the present paper concentrate attention on rough wall flows which more or less exclusively prevail in the geophysical environment. There is every reason to expect that horseshoe-type vortical structures also represent the dominant feature of boundary layer structure over rough walls and therefore the smooth wall observations remain highly relevant.

Results from two independent experimental studies are presented. For ease of reference these are simply termed 'experiment A' and 'experiment B'. The primary objective of experiment A was to try and establish the three-dimensional form of the turbulence structures linked to the ejection and inrush events observed over rough walls in the preceding investigation by Grass (1971). Based on the findings from this earlier study, Grass suggested that the near-wall turbulence structures should scale with the size of the wall roughness elements. Perry & Chong (1982) adopted this suggestion in extending their hierarchy model to rough wall flows and scaling their first hierarchy of vortical structures in direct proportion to the roughness dimension. Experiment B is concerned with measuring the actual spanwise scale of the near-wall structures for boundary conditions ranging from hydrodynamically smooth to fully rough. This investigation also addresses the intriguing question of whether or not the equivalent of viscous sublayer streaks exist over rough walls. Apart from the direct relevance to the important hierarchy model, such information yields valuable insight into the complex mechanics of wall-layer flows in general.

PHILOSOPHICAL TRANSACTIONS OF THE ROYAL SOCIETY A MATHEMATICAL, PHYSICAL & ENGINEERING SCIENCES

Table 1. *Flow and bed roughness conditions and derived variables*

experiment	A	B			
	2D strip roughness	hydro-dynamically	spherical roughness		
bed roughness condition	$k = 5$ mm	smooth	$k = 1.15$	$k = 6$ mm	$k = 12$ mm
flow depth (relative to velocity origin D/mm)	54.5	50.3	49.9	48.9	49.6
depth average velocity, U/(mm s^{-1})	144	105	106	111	106
kinematic viscosity, ν/(mm^2 s^{-1})	0.97	0.94	0.94	1.05	1.03
Reynolds number, DU/ν	8076	5613	5611	5160	5114
bed shear velocity, U_τ/(mm s^{-1})	16.1	6.07	6.46	8.48	9.21
Karman constant, K	0.37	0.395	0.387	0.384	0.382
roughness height, k/mm	5	—	1.15	6	12
kU_τ/ν	83.0	—	7.9	48.5	107.3
height of velocity origin above baseplate datum/mm	1.4	—	0.70	4.8	9.4
roughness length scale, y_0/mm	0.96	—	0.025	0.169	0.327
$k_s = 30/y_0$	28.7	—	0.78	5.07	9.82
$k_s U_\tau/\nu$	476.4	—	5.4	40.9	79.2
k_s/k	5.74	—	0.68	0.85	0.82
measurement height above roughness y_1/mm	—	1	1	3	3.5 0.5
λ/mm	—	15.6	16.1	19.5	38.2 12.0
$\lambda U_\tau/\nu$	—	101	110	158	340 107
λ/k	—	—	14.0	3.25	3.18 1.0

Indeed, a central objective of all these basic studies is to provide an improved understanding of the fundamental physics of boundary layer turbulence. Such knowledge is an essential prerequisite for the development of improved turbulence models. The success of this approach is demonstrated by the encouraging progress reflected in the models proposed, for example, by Perry *et al.* (1986), Walker *et al.* (1989) and Piomelli *et al.* (1989).

2. Experimental arrangements and procedure

Experiment A

Measurements were made in a fully developed turbulent boundary layer formed on the rough bed of an open channel water flow. The glass-sided channel was 0.5 m wide and 6.2 m long, and the uniform flow depth was approximately 50 mm. Bed roughness comprised parallel spanwise strips of 5 mm square section brass rod, with a gap width of 20 mm, stuck to a glass bed plate. This 'k-type' roughness arrangement was chosen because of its simplicity and reproducibility, and its well-documented properties (Perry & Joubert 1963; Perry *et al.* 1969). The regular geometry also greatly facilitated successful implementation of the three-dimensional measurement technique.

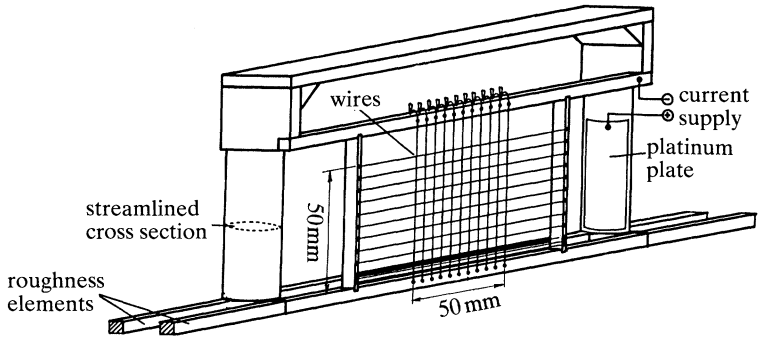

Figure 2. Cross-wire electrode system used to generate an orthogonal grid of hydrogen bubble tracer lines.

Great care was taken with the design of the channel inlet system to eliminate flow disturbances and provide a closely uniform, low turbulence approach flow at the channel entrance which coincided with the leading edge of the bed plate. The measurement station was located 2 m downstream at a position where the flow was fully developed but remained suitably two dimensional. Water was recirculated through the channel via a constant head tank which maintained very steady flow conditions. Depth average flow velocity and corresponding Reynolds number data are given in table 1. A laser doppler anemometer was used for the general control measurements and to obtain the mean velocity profile and long-term averaged turbulence characteristics.

The main emphasis of the experimental programme centred on the successful design and deployment of a novel measurement system for approximate determination of the quasi-instantaneous velocity vector field throughout three-dimensional blocks of flow space. This technique was based on an adaptation of the hydrogen bubble tracer method previously described by Grass (1971). The single bubble-generating wire used in the earlier tests was replaced with a grid of orthogonal 25 μm diameter wires in a vertical plane perpendicular to the flow direction, as illustrated in figure 2. A negative voltage, pulsed at 20 Hz, was applied to the wire electrodes. This released 20 regular grid patterns of bubble tracers, comprising 132 node points into the flow every second. A high-speed motion camera running at 200 frames per second was used in conjunction with the stereoscopic viewing system illustrated in figure 3 to record the progress of the tracer grids as they were swept downstream. The hydrogen bubbles were illuminated by an intense narrow strip of light which ensured that only one tracer grid appeared in the field of view at any instant in time, to avoid visual confusion. A typical film-frame showing stereoscopic images of the illuminated bubble tracer grids and the generating wires is reproduced in figure 4. The grid wire spacing was 5 mm, except in the zone of high velocity gradient close to the bed, where it was reduced to 2 mm in the vertical direction as indicated in figures 2 and 4.

A film coordinate analyser was used to measure the distance the tracer grid node points moved in an interval of $\frac{1}{100}$ s. These data were then processed by computer, making due allowance for perspective distortion and the wake velocity defect behind the generating wire (Grass 1971), to yield 132 simultaneously measured values of the three-dimensional velocity vector across a 50 mm × 50 mm area in the centre of the channel. These velocity vector matrices were updated every $\frac{1}{20}$ s, and Taylor's

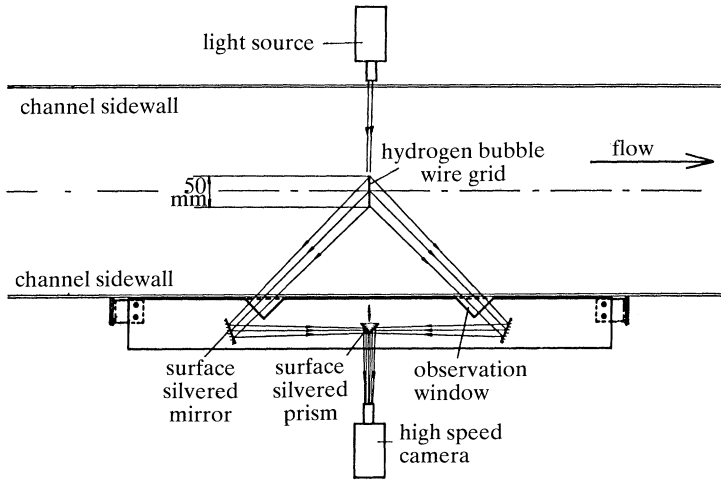

Figure 3. Stereoscopic photographic system.

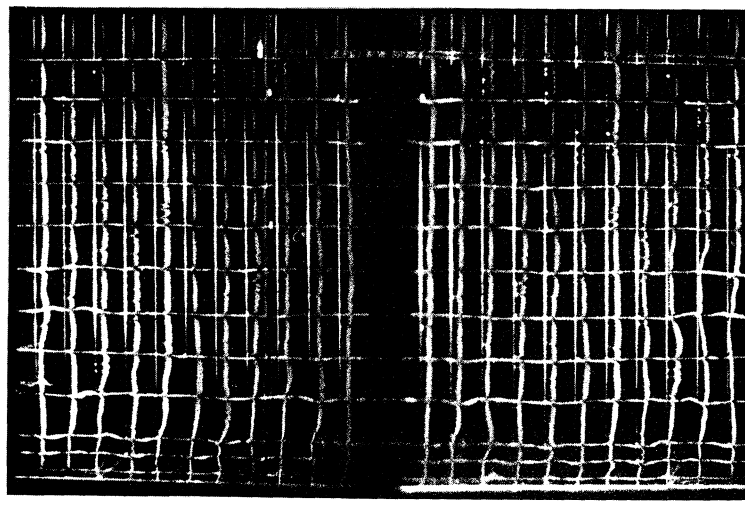

Figure 4. Typical film frame showing stereoscopic images of the hydrogen bubble tracer grids.

'frozen-eddy' hypothesis (Taylor 1938) was used to generate an approximate picture of the quasi-instantaneous three-dimensional velocity field throughout blocks of the flow space swept through the measuring grid. The resulting three-dimensional velocity data matrix was then used to compute the corresponding vorticity field. This allowed vortex-lines to be traced out through the three-dimensional flow field as a powerful means of identifying the presence, and delineating the geometry of, vortical or other structural forms embedded in the boundary layer. A detailed description of the experimental arrangements and measurement techniques used in the 'Experiment A' study is given by Stuart (1984).

Experiment B

The Experiment B test programme was carried out using the same water channel and general fully developed, uniform flow conditions as in Experiment A, also maintaining the same flow depth of *ca.* 50 mm. The bed roughness condition was,

however, varied in these tests from hydrodynamically smooth to fully rough. This was achieved using a range of different diameter glass spheres, randomly packed in a single layer resting on the glass bed plate. Laser doppler anemometry was used for the general control measurements.

The main measurements, concerned with investigating the spanwise structure of the near-wall turbulence, once again used the hydrogen bubble tracer technique. The general arrangement was, however, very much simpler than in Experiment A, and comprised a single, horizontal, bubble-generating wire located at variable height close to the bed. A pulsed negative voltage was supplied to this wire electrode, releasing thin lines of bubble tracers into the illuminated near-bed flow field. These tracer lines were photographed through a viewing plate just touching the free water surface, using a still 35 mm camera. Sample photographs are shown in figure 17 for the different bed roughness conditions. As can be seen, the newly released tracer lines retain coherence along their entire length. A coordinate analyser was used to define the shape of these coherent tracer lines in digital format for spatial spectrum analysis. Ensemble averages, based on 35 individual spectra were calculated to establish the existence or otherwise of any preferred spanwise wavelength and to measure such wavelengths from the spectral peaks. In the case of the smooth wall test, the mean spacing of the low-speed streaks in the viscous sublayer was also determined by direct measurement using a marking technique similar to that adopted by Smith & Metzler (1983). It was found that this method gave closely similar results, confirming that the two approaches are basically focusing on the same physical flow feature. However, direct measurement becomes excessively subjective over rough walls because of the loss of streamwise streak coherence. The 'Experiment B' investigation is ongoing at the time of writing, and only preliminary results of direct relevance to the present discussion are presented below.

3. Results and discussion

Considering the Experiment A results first, the long-term average mean velocity and normal and shear components of the Reynolds stresses were measured using a laser doppler anemometer for comparison with previous work and to derive relevant scaling parameters. As expected the two-dimensional strip roughness behaved as conventional 'k-type' roughness, following the terminology and in-line with the findings of Perry & Joubert (1963). The measured streamwise and vertical components of turbulence intensity, were in very close agreement with corresponding data obtained in similar open channel flows over beds with three-dimensional roughness elements by Grass (1971), Nezu (1977) and Raven (1977).

The mean velocity profile, measured in the centre of the channel at the test location, is shown in relation to the bed roughness elements and the free water surface in figure 5. This particular set of data was measured above the centre line of one of the roughness strips. The effective velocity origin was determined using a combination of the progressive origin shift method suggested by Clauser (1956) and adapted by Perry & Joubert (1963), and linear regression to obtain the best fit straight line in the logarithmic zone. This inevitably somewhat subjective process, located the velocity origin 1.4 mm above the surface of the glass base plate and 3.6 mm below the tops of the roughness elements as shown in figure 5. This result is in close agreement with the corresponding origin locations derived and quoted by Perry & Joubert (1963) and Perry *et al.* (1969). A semi-logarithmic plot of the mean

Figure 5

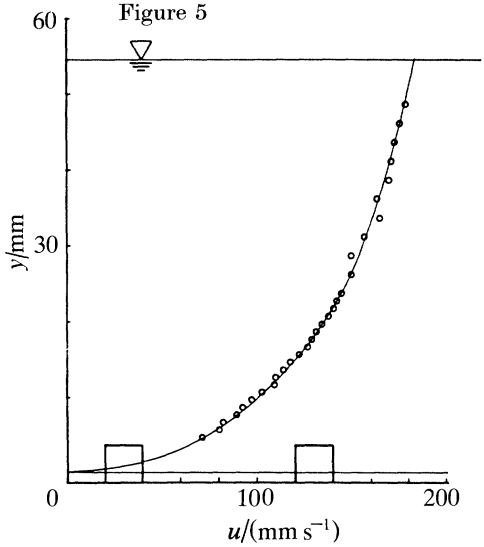

Figure 6

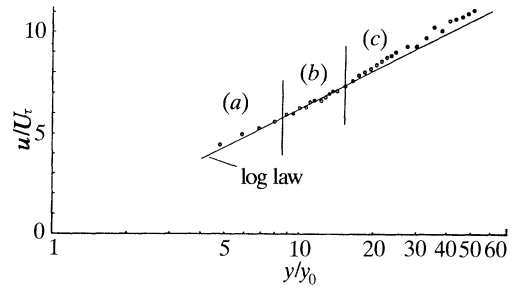

Figure 5. Mean velocity profile in relation to the bed roughness elements and the free water surface.

Figure 6. Mean velocity profile scaled by shear velocity, U_τ and roughness length y_0. (*a*) Roughness layer, (*b*) logarithmic layer, (*c*) wake zone.

velocity data, using this shifted origin, is presented in figure 6, and exhibits the conventional roughness layer, logarithmic layer and wake zone regions. The roughness length scale, y_0, appearing in figure 6 was derived from the intercept of the 'best fit' logarithmic layer straight line with the y axis. Average values of mean velocity data measured respectively above the roughness element centre line and over the centre line of the gap between the roughness elements was used in this extrapolation procedure. Small systematic differences in the two sets of data were only apparent out to approximately 3 mm above the tops of the roughness strips.

The bed shear stress and hence the bed shear velocity, U_τ, were obtained by extrapolating the linear total shear stress distribution, obtained by adding the Reynolds shear stress and viscous shear contributions, back to the bed. Derived values of the relevant scaling parameters and general flow and bed roughness characteristics are given in table 1. If, following Nikuradse (1933), we consider an equivalent sand, or in the present case gravel size, k_s, to produce the same degree of roughness, putting $y_0 = \frac{1}{30}k_s = 0.96$ mm (from table 1) we find that $k_s/k = 5.74$ (where k denotes the roughness strip height = 5 mm). In comparison, the 12 mm diameter spherical roughness used in the Experiment B test yields a modest and expected k_s/k value of 0.82 (table 1). These findings demonstrate that the two-dimensional strips produce a very rough boundary condition. The high k_s/k ratio agrees well with corresponding values for similar two-dimensional roughness elements quoted in a detailed review by Yaglom (1979). Equally large k_s/k values are also recorded for three-dimensional roughness elements which are not closely packed together. Yaglom (1979) also discusses some interesting early measurements by Paeschke (1937) who obtained k_s/k values of approximately 4 in wind flow over ordinary grass cover and for many other agricultural crops including beets.

Hydrogen bubble tracers generated on a single vertical wire, were used for general dynamic flow visualization recorded using high speed motion photography. A typical frame from the resulting film is shown in figure 7. All the characteristic features of

PHILOSOPHICAL TRANSACTIONS OF THE ROYAL SOCIETY A MATHEMATICAL, PHYSICAL & ENGINEERING SCIENCES

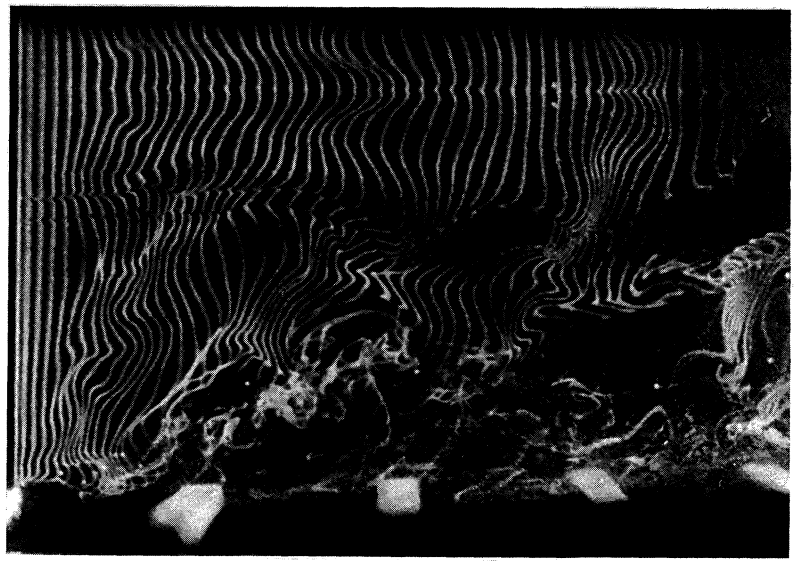

Figure 7. Hydrogen bubble visualization of general flow structure.

rough wall turbulence including violent eruptive ejection of fluid from the near bed region and energetic inrush events bringing high velocity fluid in towards the wall, observed in the earlier study using three-dimensional pebble roughness (Grass 1971) were clearly visible in the flow over the two-dimensional strip roughness. Roll-up of spanwise and streamwise vorticity, to some extent identifiable in figure 7, were clearly apparent in the moving images, as they developed in time.

The considerable manual effort involved in abstracting tracer coordinate data from the stereoscopic film images for the three-dimensional analysis inevitably imposed restrictions on the application of the technique. A high level of concentration is demanded of the system operator coupled with good interpretative skills when, for example, the hydrogen bubble tracer quality perhaps deteriorates locally due to contamination of the electrode wire surface. The process is also extremely time consuming. With the 132 node points and 20 Hz sampling rate used in the present study it took in the region of 15–20 h of film analysis time to generate three-dimensional data for 1 s of swept flow space. Set against these draw backs, however, is the extraordinary power and potential of this novel technique which effectively generates data crudely equivalent to 132 triple-channel laser doppler anemometers working simultaneously! It is undoubtably the case that linked to automated data acquisition systems, flow tracer methods such as the one presented here and alternative particle image velocimetry (PIV) approaches, open up exciting new opportunities for physical experimentation to parallel developments in the numerical simulation area.

However, given the manually based techniques available in the present investigation, it was clearly essential to carefully select the blocks of swept flow space subjected to full three-dimensional analysis to make best use of the severely restricted sampling time. Some method of previewing the general state of the field was therefore required to establish periods when interesting events appeared to be occurring. This conditional sampling was achieved by initially carrying out a two-dimensional analysis, using the hydrogen bubble tracers released from the vertical

PHILOSOPHICAL TRANSACTIONS OF THE ROYAL SOCIETY A MATHEMATICAL, PHYSICAL & ENGINEERING SCIENCES

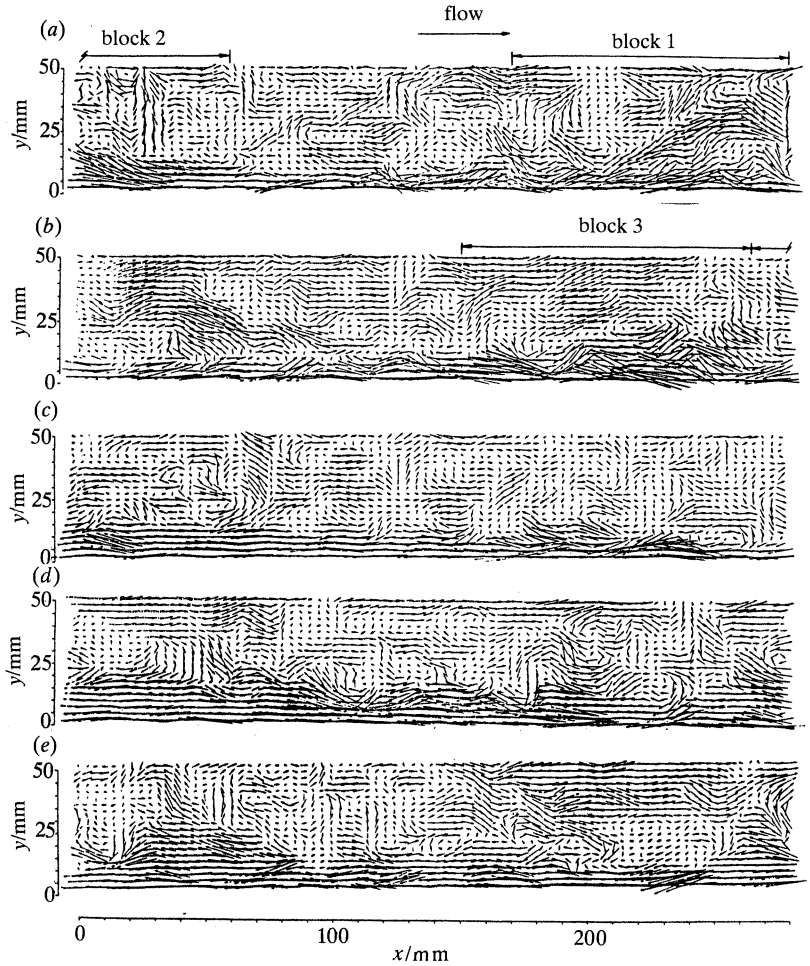

Figure 8. Centre line ($u-Uc$, v) velocity vector plots in convected reference frame.

centre-line wire only, to measure instantaneous profiles of streamwise velocity, u, and vertical velocity, v, updated every $\frac{1}{20}$ s. Taylor's hypothesis was then used with an assumed convection velocity equal to the depth averaged mean velocity $U_c = 144$ mm s^{-1}, obtained from the laser measurements, to generate the ($u-U_c$, v) vector plot segments shown in figure 8. Additional velocity vectors have been inserted in these diagrams half way between the measured vectors using nonlinear interpolation routines, to improve structural detail. Each consecutive segment represents 2 s flow time, 10 s in total.

The figure 8 diagrams give a convected view impression of the instantaneous streamline patterns as seen by an observer travelling with the flow at the depth averaged velocity, U_c. Cross sections through transverse vortices of varying size and strength, inclined internal shear layers, and ejection and inrush zones are clearly visible in the flow structure. For example, note: the vortex sections centred on ($x = 145$ mm, $y = 20$ mm) Segment 1 and ($x = 220$ mm, $y = 25$ mm) Segment 2; the shear layer located at ($x = 240$ mm, $y = 30$ mm) Segment 1; and the ejection and inrush events located at ($x = 10$ mm, $y = 10$ mm) Segment 1 and ($x = 270$ mm,

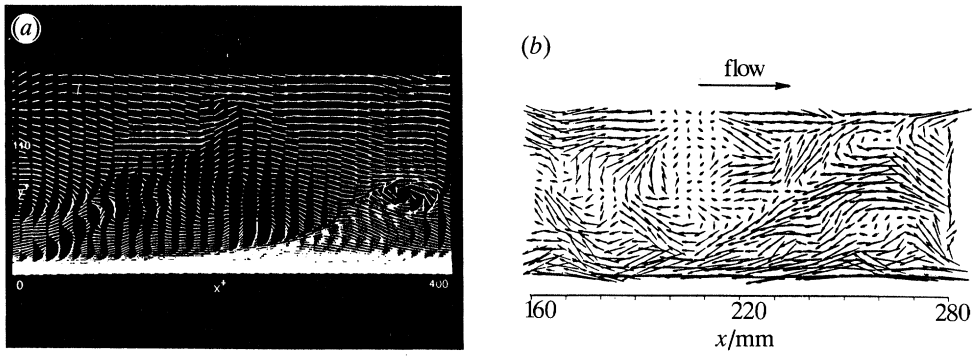

Figure 9. Examples of shear layer roll-up with section through transverse 'head' vortex. (*a*) Numerical stimulation of smooth wall boundary layer (Robinson *et al.* 1989). (*b*) Present rough wall study (segment 1, figure 8).

$y = 5$ mm) Segment 2 respectively. The original versions of the velocity vector diagrams in figure 8 were colour coded according to whether the local streamwise velocity component was greater or less than the local mean value. Ejection events thus appeared as black and inrush events as red groupings of velocity vectors. Identification of these dominant Reynolds shear stress and turbulence production events in the figure 8 segments was also facilitated by inspection of the instantaneous Reynolds shear stress profiles calculated from the instantaneous (u, v) velocity distributions.

Three sections of the figure 8 velocity vector segments were selected on the basis of apparently relevant structural content, for full three-dimensional analysis. These are referred to as Blocks 1, 2 and 3 (figure 8). With reference to the previously quoted examples, Block 1 includes the Segment 1 shear layer structure; Block 2, the Segment 1 ejection event, which is linked to high measured Reynolds shear stress; and Block 3, the Segment 2, vortex section associated with an extremely active, underlying ejection zone at the bed.

The Block 1 shear layer is reproduced at larger scale in figure 9. As can be seen there is a clear indication of vortex roll-up at the top of the layer. Also reproduced in figure 9, is a corresponding velocity vector representation of the shear layer example presented by Robinson *et al.* (1989) derived from numerical simulation of a turbulent boundary layer. The detailed matching between these two flow field patterns is quite remarkable with the velocity vectors surrounding the rolled-up vortex head and the upstream stagnation point closely reproduced in both direction and magnitude. Even the large diamond-shaped areas, upstream of the shear layer, with a core velocity apparently more or less equal to the viewing frame convection velocity, show distinct similarity. This certainly suggests a close identity between the three-dimensional flow structures generating these velocity patterns over a completely smooth and a fully rough boundary. The fact that the general flow pattern associated with the shear layers illustrated in figure 8, also recurs in the ensemble averaged patterns of large-scale structure produced by Thomas & Brown (1977) for example, adds support to the concept of a vortical generating structure of basically universal geometry, but following a scale hierarchy, as suggested by Perry & Chong (1982).

It is apparent from the above discussion, that two-dimensional velocity vector representations on sliced planes through the flow field are extremely effective in

PHILOSOPHICAL TRANSACTIONS OF THE ROYAL SOCIETY A MATHEMATICAL, PHYSICAL & ENGINEERING SCIENCES

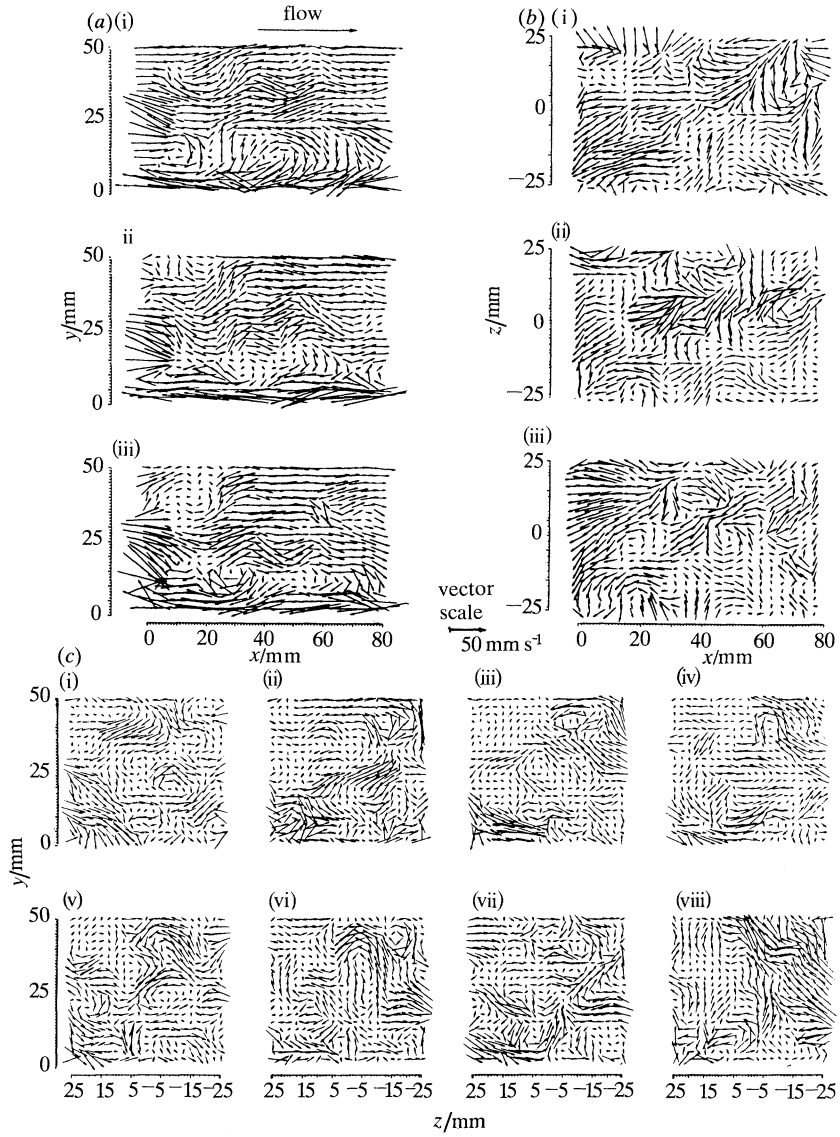

Figure 10. Examples of velocity vector plots from three-dimensional Block 2. (*a*) $(u-U_c, v)$ vectors in (x, y) planes, $z = 25$(i), 20(ii), 15(iii); (*b*) $((u-U_c), w)$ vectors in (x, z) planes, $y = 50$(i), 45(ii), 40(iii); (*c*) v, w vectors in (y, z) planes, $x = 79.2$(i), 72(ii), 64.8(iii), 57.6(iv), 50.4(v), 43.2(vi), 36(vii), 28.8(viii). All values in millimetres.

revealing the presence and form of relevant structural features. The three-dimensional analysis provided three-component velocity vector data throughout the swept volumes of Blocks 1, 2 and 3. This permits a whole series of velocity vector plots to be produced for different vertical streamwise, vertical cross flow and horizontal planes. Examples of these 'slice' representations of the velocity field are shown in figure 10 for the Block 2 results. Because of the vertical mean velocity gradient it is necessary to vary the convection velocity for the plots in the horizontal (x, z) plane. It was found that using the mean streamwise velocity at the level of the

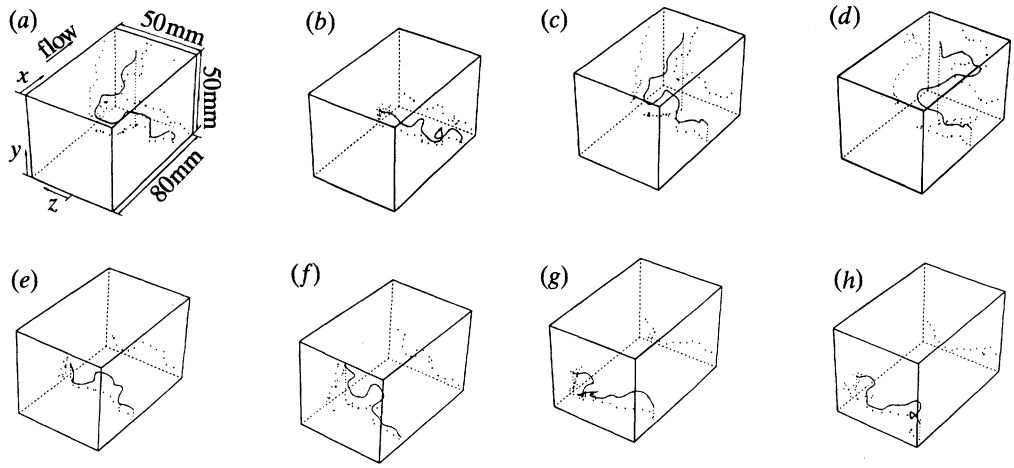

Figure 11. Typical single vortex-line plots for Block 2 (figure 8). Tracking origin in plane $y = 7.5$ mm.

plane height above the bed, gave satisfactory results as indicated in figure 10*b*. Once again vortex sections can be identified in all three planes. These three-dimensional representations are additionally valuable since they permit assessment of the extent of spacial coherence in the observed structures. The original plots were again colour coded to identify zones where the streamwise velocity component was either greater or less than the local mean velocity.

The Block 2 vorticity field was explored first. This was carried out in a comprehensive and systematic manner, initially ignoring the information obtained from the velocity vector plots concerning the presence, form and location of any coherent structure. Single vortex lines were tracked from over 200 starting points spread in a regular grid pattern throughout the block. Examples of these vortex lines with starting points located in horizontal planes 7.5 mm, 15 mm and 30 mm above the tops of the roughness strips are presented in figures 11, 12 and 13 respectively. The most surprising feature of these single vortex lines is their extraordinary coherent, untangled form. This finding is particularly surprising if one observes the apparently relatively advanced state of chaos existing in the near wall flow field visualized in figure 7. Dominant vorticity in the flow field is clearly associated with relatively young and coherent flow structures. Vortex lines transported long distances in old contorted structures would presumably exhibit a much more tangled form. While examples of tangled vortex lines were found amongst the very large sample they represented a small percentage and the vortex lines in figures 11–13 are typical. The fact that the vortex lines often span between the wall and the flow surface and yet remain within the confines of the measurement volume under the action of the velocity gradient, suggests that the transport across the boundary layer has been relatively rapid. It also suggests that the structures responsible for such transport must be of a scale commensurate with the boundary-layer thickness or flow depth.

Because of the relatively coarse measurement grid spacing, there was some concern regarding the reliability of the vortex lines. While this inevitably involved some small-scale filtering, it was felt that with the interpolation procedures adopted, the tracking technique was capable of following the dominant vorticity paths through

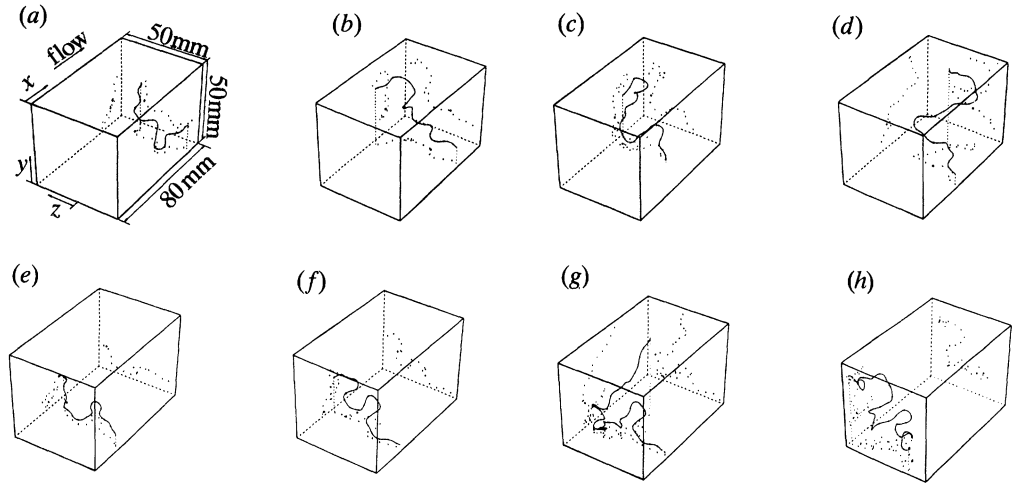

Figure 12. Typical single vortex-line plots for Block 2 (figure 8). Tracking origin in plane $y = 15$ mm.

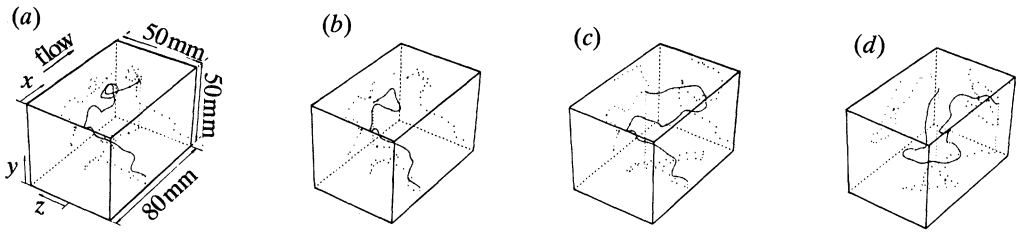

Figure 13. Typical single vortex-line plots for Block 2 (figure 8). Tracking origin in plane $y = 30$ mm.

the fluid. Tests were carried out to optimize the length of the vector step advance used in the tracking procedure. A step length of 0.5 mm was selected for the main analysis on the basis that it gave very satisfactory reproducibility of vortex line traces in reverse-tracking tests.

To give a clearer impression of the three-dimensional form of the vortex-lines, their projected images are plotted on the block side walls and base. As expected, the side wall projections invariably indicate downstream inclination which in turn implies strong vortex stretching and energy absorption from the mean flow field. Horseshoe-shaped loops are also very common features of these single vortex lines. While such features can be formed by a lifted shear layer and may not be indicative of a rolled-up horseshoe vortex, an important point correctly elaborated by Kline & Robinson (1989) and Robinson (1989), they can be taken as a possible indication of the presence and location of such structures for further investigation using multiple vortex lines. Such lines also represent a lagrangian, integrated history of the movement of the fluid particles constituting the line, or in its near vicinity, subsequent to their being lifted away from the vorticity generating zone at the wall (Lighthill 1979). Even in a passive role as flow tracer, therefore, vortex lines give valuable information about the recent local structure of the flow.

It was anticipated that vortex lines started from tracking origins close to the bed would tend to pick up the most recently generated small-scale vortical structures

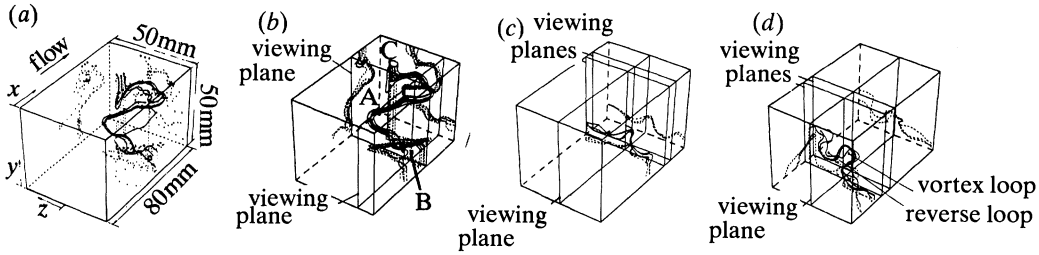

Figure 14. Multiple vortex-line plots revealing vortical and coherent structures in Block 2 (figure 8) flow field.

forming in the intense shear layers separating from the roughness elements. These shear layers are strongly three-dimensional due to the violently disturbed nature of the approach flow. This is confirmed by the preponderance of smaller scale loops in vortex lines remaining close to the wall in figure 11 compared with figures 12 and 13. Perhaps the most significant qualitative impression given by these single vortex lines is of a flow dominated by coherent powerful new structures which all connect back to the vorticity generation zone at the wall and which increase in size with wall distance. This observation is entirely consistent with Townsend's attached-eddy hypothesis used as a basis for their model by Perry & Chong (1982).

The fact that many of these looping, single vortex lines are embedded in rolled-up vortical structures was demonstrated by multiple line tracking. The resulting vortex line bundles are shown in figure 14*c* and *d* corresponding to figure 11*b* and *f*. The splendid example of a near bed, horseshoe vortex in figure 14*d*, is directly linked to the ejection event located at coordinate point ($x = 10$ mm, $y = 10$ mm) in Segment 1, figure 8. This ejection event is also marked by the outward (v, w) velocity vectors in the cross-flow plane located at ($x = 36$ mm, $y = 10$ mm, $z = 0$ mm) in figure 10*c*. Fluid is being pulled up and ejected between the side legs of this horseshoe vortex. Vortex line patterns are also observed to closely repeat for different starting points as for example in figure 11*f* and 12*f* and figures 11*d*, 12*d* and 13*c*. This is again a positive indication of the presence of powerful rolled-up vortices embedded in the flow which have a relatively large 'catchment area' for tracking start points. It also demonstrates that given the presence of such a structure, the tracking technique used is capable of tracing out vortex lines through it rather than generating random spacial patterns.

These arguments are borne out by the multiple vortex line delineation of the spectacular snaking vortex displayed in figure 14*a* and *b*. This vortex loops its way upwards across the entire thickness of the boundary layer and terminates in a loose, broken end at the free surface. Whirlpool marks are a commonly observed surface feature of river flows and undoubtably result from the draw down effect of such free vortex ends. These loose vortex ends are presumably created when lifted shear layers and rolled-up vortical structures closely approach the free-surface boundary, fracture and attach themselves to the surface. The interaction of vortical structures with the free-surface boundary is also linked to the formation of surface boils discussed by Grass (1971), Jackson (1976) and Muller & Gyr (1986).

Vortex cross sections marked A, B and C in figure 14*b* are discernible in the velocity vector plots in figure 10. Streamwise cross section A, is located at approximate coordinate position ($x = 50.4$ mm, $y = 25$ mm, $z = 5$ mm) in figure 10*c*, spanwise cross section B at ($x = 30$ mm, $y = 15$ mm, $z = 15$ mm) in figure 10*a*, and

PHILOSOPHICAL TRANSACTIONS OF THE ROYAL SOCIETY A MATHEMATICAL, PHYSICAL & ENGINEERING SCIENCES

the free-surface horizontal cross section at ($x = 70$ mm, $y = 50$ mm, $z = 5$ mm) in figure 10*b*. This strong correlation and coincidence between vortex line and velocity vector representations, reinforces confidence in the reality of these vortical structures.

Further examples of multiple vortex line displays are presented in figure 15. Once again these plots demonstrate clear coherence in the flow structure and provide additional direct evidence of the presence of vortical structures with a general horseshoe-type configuration and with a wide range of scales. The plots in figure 15*a–d* are for Block 1 which was selected for three-dimensional analysis because of the interesting shear layer revealed by the centre line velocity vector plots (figures 8 and 9*b*). The colour coding in the three-dimensional velocity vector representations confirms that the fluid particle velocities above and below this shear layer are respectively higher and lower than the local mean values. These velocity vector plots also show that the rolled-up vortex visible at the top of the shear layer in figure 9*b* spans approximately two thirds of the block width and is associated with strong perturbations in the underlying flow field. Vortex line plots confirm the spanwise coherence of this vortex.

Figure 15*d* shows the five vortex lines started at points located along the centre of the shear layer (figure 9*b*). These lines demonstrate that the shear layer has large spanwise coherence and also that it has a steep cross-flow inclination at the upstream end. This spanwise slope is clearly shown in the end wall projection of the vortex line bundle traced out in figure 15*c*. The corresponding projection of this bundle on the side wall shows that it is only very slightly inclined in the downstream direction. This suggests very rapid lifting of the vortex lines by a strong upwelling of the underlying fluid. The colour-coded velocity vector plots confirm that a violent ejection event associated with large Reynolds stress production, is indeed responsible. Such powerful eruptions, which lift fluid almost vertically away from the wall are a characteristic feature of near wall turbulence over very rough boundaries, as previously discussed by Grass (1971), and observed in the general flow visualization films produced in the present study.

The multiple vortex line plot in figure 15*b* was tracked from the position of a streamwise vortex identified in the cross-flow plane velocity vector diagrams. While the individual vortex lines become somewhat dispersed with distance from the 'necked' start position, and have all the appearance of tentacles, they nevertheless retain considerable overall cohesion and collectively trace out the general shape of part of a horseshoe structure. In contrast to the figure 15*c* structure, this looped configuration has a very shallow angle of inclination to the flow direction. This suggests that it forms part of a relatively old and highly stretched vortex. It is interesting to note that the eruption zone, previously discussed, lies just upstream of the figure 15*b* structure.

Block 3 was selected for three-dimensional analysis on the basis of the vortex cross-section identified at position ($x = 220$ mm, $y = 25$ mm) in Segment 2 of figure 8 and the active underlying ejection zone. The three-dimensional velocity vector diagrams and the vortex line bundle presented in figure 15*f*, show that the present vortex spans the entire block width and takes the form of a looped structure arching upwards from the wall. This is directly linked to strong ejection events and associated high Reynolds stress production just upstream of the vortex. Evidence of other horseshoe-shaped vortical structures embedded in the Block 3 flow space is presented in figures 15*e*, *g*, *h*.

PHILOSOPHICAL TRANSACTIONS OF THE ROYAL SOCIETY A MATHEMATICAL, PHYSICAL & ENGINEERING SCIENCES

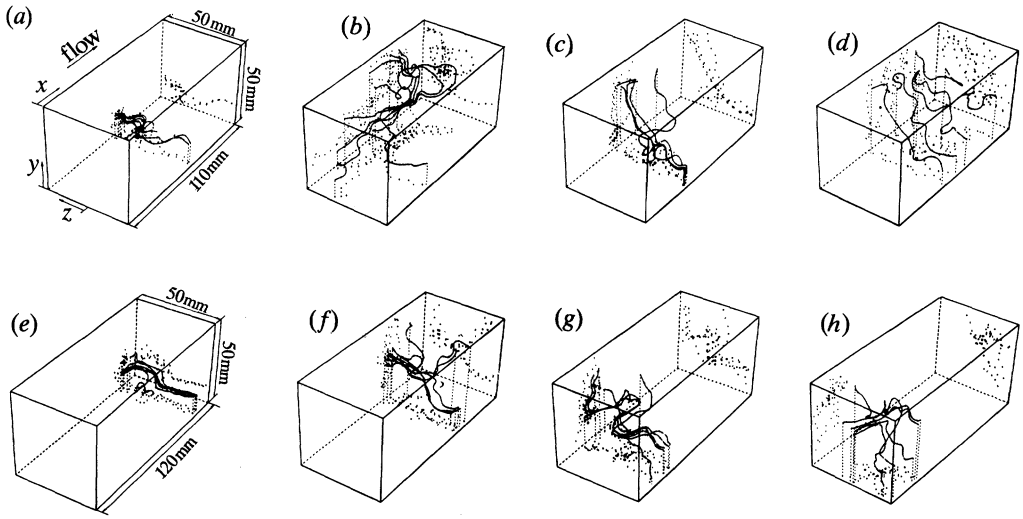

Figure 15. Multiple vortex-line plots revealing vortical and coherent structures in Blocks 1 (*a*)–(*d*) and 3 (*e*)–(*h*) (figure 8) flow fields.

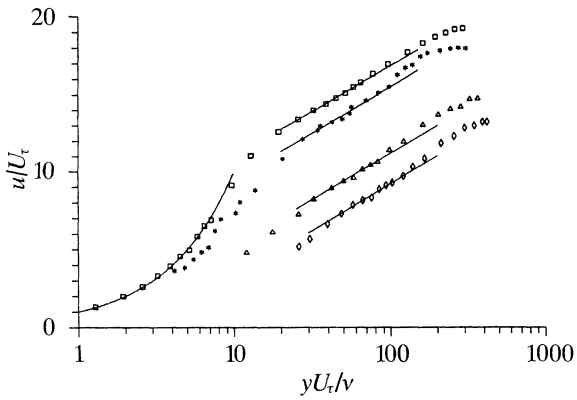

Figure 16. Mean velocity profiles scaled by smooth-wall variables for different boundary roughness conditions, Experiment B. □, smooth; *, △, $k = 1.15$ mm; △, $k = 6$ mm; ◇, $k = 12$ mm.

To conclude this discussion of the 'Experiment A' results therefore, it is self-evident that the presence of vortical structures such as those depicted, for example, in figures 14*b* and 15*b*, with their massive potential for absorption of mean flow energy through the stretching mechanism and their capacity to induce strong three-dimensional currents and hence generate large contributions to Reynolds shear stress, must play a critical role in turbulent boundary layer dynamics. This key role has perhaps been best summed up by Kuchemann (1965) who described vortices as 'the sinews and muscles of fluid motions'.

Turning now briefly to the preliminary Experiment B results, the mean velocity profiles for the four different wall roughness conditions and for the same flows depicted in the figure 17 visualization photographs, are presented in figure 16. These exhibit the normal logarithmic and wake zone characteristics as in the case of the profile for the two-dimensionally strip roughness (figure 8). Plotted in terms of the

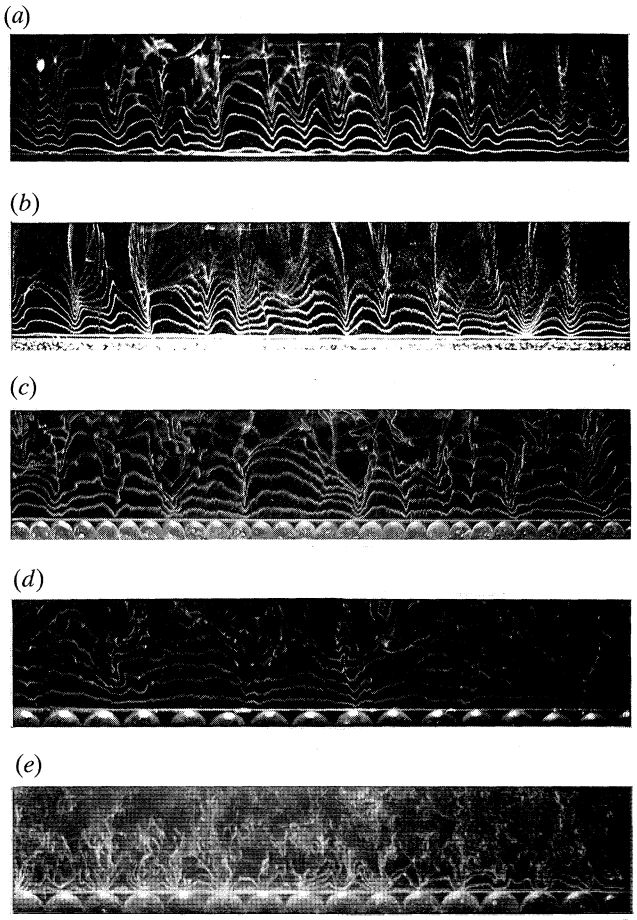

Figure 17. Near wall flow structure visualized by hydrogen bubble tracers generated on transverse wire parallel to the bed. Bed roughness conditions and wire distance from top of roughness, y_1, as follows: (*a*) smooth: $y_1 = 1$ mm; (*b*) $k = 1.15$ mm, $y_1 = 1$ mm; (*c*) $k = 6$ mm, $y_1 = 3$ mm; (*d*) $k = 12$ mm, $y_1 = 3.5$ mm; (*e*) $k = 12$ mm, $y_1 = 0.55$ mm.

smooth wall viscous length scale the velocity profiles also show the standard pattern of roughness velocity defect relative to the smooth wall profile. This defect increases with increasing wall roughness. The general flow conditions and values of derived parameters such as the bed shear velocity, U_τ, and the roughness length scale, y_0, are set out in table 1. Roughness Reynolds numbers, $U_\tau k/\nu$, are also quoted in table 1 and indicate that under these particular flow conditions, the 1.15 mm diameter spheres lie in the lower transitional roughness régime, the 6 mm spheres in the upper transitional régime and the 12 mm spheres in the fully rough régime.

The smooth wall visualization photograph in figure 17*a* clearly illustrates the extensive coherence of the low speed streaks in the streamwise direction. Similar coherence is seen to persist for the 1.15 mm diameter roughness (figure 17*b*) reflecting the continued dominance of viscous shear transfer at the wall. These low velocity ejection zones are still apparent in the near wall layer flow over the 6 mm diameter spheres. However, as illustrated in the figure 17*c* photograph, their general characteristics have now changed significantly. The distance between the zones has

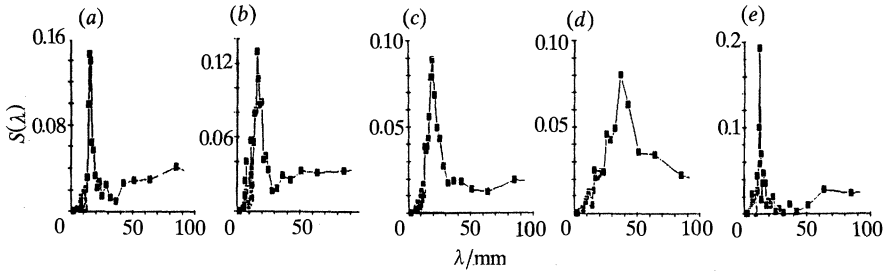

Figure 18. Ensemble averages of transverse wavelength spectra of spanwise velocity fluctuations derived from hydrogen bubble tracers as illustrated in figure 17. Flow conditions and y_1 values of (*a*)–(*e*) correspond with figure 17*a*–*e*, respectively.

clearly increased as has their width, while their streamwise coherence is substantially reduced. These trends are further advanced in the case of the fully rough 12 mm diameter spheres.

A remarkable feature of the rough wall flow is its apparent ability to order itself very rapidly over a small vertical distance above the tops of the roughness elements. This is demonstrated by contrasting the near bed flow field characteristics visualized in figure 17*d* and *e*. In figure 17*e*, the hydrogen bubble wire is located 0.5 mm above the tops of the spheres. At this height the bubble tracers respond to the three-dimensional velocity field and pick up the intense small-scale disturbances in the separating flow round the individual roughness elements. The visualization traces show very little evidence of this highly disturbed flow state with the wire raised to just 3.5 mm above the tops of the 12 mm diameter spheres as shown in figure 17*d*.

Ensemble averaged spectra for the spanwise velocity fluctuations, corresponding to the mean flow and bed roughness conditions in figure 17*a*–*e* are presented in figure 18*a*–*e*. As can be seen, these spectra exhibit a well defined single peak which indicates the presence of a dominant spanwise wavelength, λ, in the near wall structure. The ability of the spectral peak method to pick out a preferred wavelength in the velocity perturbations, is confirmed by the measured value of 12 mm with the hydrogen bubble wire 0.5 mm above the roughness tops as in figure 17*e*. This wavelength exactly coincides with the sphere diameter as expected. In the case of the smooth wall flow, $\lambda^+ = \lambda U_\tau/\nu = 101$, in good agreement with previous measurements (see, for example, Smith & Metzler 1983). Corresponding values for the 1.15 mm, 6 mm and 12 mm spherical roughness conditions are $\lambda^+ = 110$, 158 and 340 respectively.

For the roughness Reynolds numbers quoted in table 1, under the present test conditions, λ should be largely independent of Reynolds number for the 6 mm and 12 mm diameter roughness elements. In these circumstances, following the suggestion of Grass (1971), λ should scale with the roughness dimension, k. In other words, $\lambda/k =$ const. for the geometrically similar roughness elements and packing used in these tests. This expectation is closely confirmed with measured λ/k values of 3.25 and 3.18 for the 6 mm and 12 mm spheres respectively (table 1). Further preliminary measurements indicate that these rough wall values remain reasonably constant within a thin layer above the bed as do the λ^+ values in the viscous sublayer over a smooth wall. Primary objectives of this continuing investigation are to establish the variation in λ values at larger wall distances and also to more fully explore the mechanisms responsible for generating these preferential spanwise wavelengths in the near wall layers.

4. Conclusions

There is now convincing evidence, particularly from recent direct numerical simulation studies, that horseshoe-type vortical structures usually with an asymmetrical or partly rolled-up form, represent the dominant dynamic element in smooth wall boundary layer turbulence. These vortices extract energy from the mean shear flow by the vortex stretching mechanism and act as pumps transporting mass, momentum, vorticity and contaminants, passive or otherwise, across the boundary layer.

The present results from the Experiment A test programme, provide evidence, based for the first time on direct physical measurements of the three-dimensional vorticity field, that horseshoe vortical structures are also a central feature and play an equally important role in rough wall flows. It is also apparent from the present observations that these structures increase in scale with increasing wall distance, consistent with Townsend's (1976) 'attached-eddy' hypothesis and Perry & Chong's (1982) eddy hierarchy model, based on Townsend's concept.

Preliminary results from the Experiment B investigation, show that just as in the case of the viscous sublayer region of smooth wall flow, a dominant spanwise wavelength occurs in the instantaneous cross-flow distribution of streamwise velocity close to the rough wall. The measurements indicate that for fully rough wall conditions, this wavelength, which reflects the typical scale of near wall vortical structures, is directly proportional to the bed roughness size. This additional new finding confirms the earlier suggestion by Grass (1971) based on qualitative observations, which was used by Perry & Chong (1982) to scale the near wall structure in extending their attached-eddy model to rough boundary flows.

The area of greatest remaining uncertainty in our knowledge and understanding of the physics of boundary layer turbulence concerns the process of growth in scale up through the eddy hierarchy from the often diminutive wall scales to the very large outer layer scales. Further work is needed at high geophysical scale Reynolds numbers and on the fundamentals of vortex interaction and vorticity field development under shear straining conditions. Direct numerical simulation techniques supported by carefully designed experiments, would appear to offer the best way forward for these essential basic studies at lower Reynolds numbers.

The authors acknowledge the support of Science and Engineering Research Council for a major part of the reported investigation.

References

Acalar, M. S. & Smith, C. R. 1987 A study of hairpin vortices in a laminar boundary layer. Part 1. Hairpin vortices generated by hemispherical protuberances. Part 2. Hairpin vortices generated by fluid injection. *J. Fluid Mech.* **175**, 1–41; 43–83.

Blackwelder, R. F. & Swearingen, J. D. 1988 The role of inflectional velocity profiles in the wall-bounded flows. *Int. Seminar on Near-Wall turbulence, Durbrovnik, Yugoslavia, May*. New York: Hemisphere.

Bradshaw, P. 1967 Inactive motion and pressure fluctuations in turbulent boundary layers. *J. Fluid Mech.* **30**, 241–258.

Clark, J. A. & Markland, E. 1971 Flow visualization in turblent boundary layers. *J. Hyd. Div. ASCE* 1653–1664.

Clauser, F. H. 1956 Turbulent boundary layer. *Adv. Appl. Mech.*, **4**, 1–51.

Corino, E. R. & Brodkey, R. S. 1969 A visual investigation of the wall region in turbulent flow. *J. Fluid Mech.* **37**, 1–30.

Cowley, S. J., Van Dommelen, L. L. & Lam, S. T. 1990 On the use of lagrangian variables in descriptions of unsteady boundary-layer separation. *Phil Trans. R. Soc. Lond.* A **333**, 343–378.

Falco, R. E. 1977 Coherent regions in the outer region of a turbulent boundary layer. *Phys. Fluids* **20**, 5124–5134.

Ferre, J. A., Mumford, J. C., Savill, A. M. & Giralt, F. 1990 Three-dimensional large-eddy motions and fine-scale activity in a plane turbulent wake. *J. Fluid Mech.* **210**, 371–414.

Gad-el-Hak, M., Blackwelder, R. E. & Riley, J. J. 1981 On the growth of turbulent regions in the laminar boundary layers. *J. Fluid Mech.* **110**, 73–95.

Grass, A. J. 1971 Structural features of turbulent flow over smooth and rough boundaries. *J. Fluid Mech.* **50**, 233–255.

Grass, A. J. 1982 The influence of boundary layer turbulence on the mechanics of sediment transport. *Proc. Euromech 156: Mechanics of Sediment Transport, Istanbul, July*. Balkema 1983, pp. 3–17.

Guezennec, Y. G., Piomelli, U. & Kim, J. 1989 On the shape and dynamics of wall structures in turbulent channel flow. *Phys. Fluids* A**1**, 764–766.

Hama, F. R. 1963 Progressive deformation of a perturbed line vortex filament. *Phys. Fluids* **6**, 526–534.

Hama, F. R. & Nutant, J. 1963 Detailed flow-field observations in the transition process in a thick boundary layer. In *Proc. 1963 Heat Transfer and Fluid Mechanics Inst.*, 77. Stanford University Press.

Head, M. R. & Bandyopadhyay, P. 1981 New aspects of turbulent boundary layer structure. *J. Fluid Mech.* **197**, 297–338.

Hon, T. L. & Walker, J. D. A. 1991 Evolution of hairpin vortices in a shear flow. *Computers Fluids*. (In the press.)

Hunt, J. C. R. 1973 A theory of turbulent flow round two-dimensional bluff bodies. *J. Fluid Mech.* **61**, 625–706.

Hunt, J. C. R. 1978 A review of the theory of rapidly distorted turbulent flows and its applications. *Fluid Dyn. Trans.* **9**, 121–152.

Jackson, R. G. 1976 Sedimentological and fluid-dynamic implications of the turbulent bursting phenomenon in geophysical flows. *J. Fluid Mech.* **77**, 531–560.

Jimenez, J. 1983 A spanwise structure in the plane shear layer. *J. Fluid Mech.* **132**, 319–336.

Kasagi, N., Hirata, M. & Nishino, K. 1986 Streamwise pseudo-vortical structures and associated vorticity in the near-wall region of a wall-bounded turbulent shear flow. *Exp. Fluids* **4**, 309.

Kim, H. T., Kline, S. J. & Reynolds, W. C. 1971 The production of turbulence near a smooth wall in a turbulent boundary layer. *J. Fluid Mech.* **50**, 133–160.

Kim, J. & Moin, P. 1986 The structure of the vorticity field in turbulent channel flow. 2. Study of ensemble-averaged fields. *J. Fluid Mech.* **162**, 389–363.

Kline, S. J., Reynolds, W. C., Schraub, F. A. & Runstadler, P. W. 1967 The structure of turbulence in boundary layers. *J. Fluid Mech.* **30**, 741–773.

Kline, S. J. & Robinson, S. K. 1989 Turbulent boundary layer structure: progress, status and challenges. *Second IUTAM Meeting on Structure of Turbulence and Drag Reduction, Zurich, July*.

Kuchemann, D. 1965 Report on the IUTAM Symposium on concentrated vortex motions in fluids. *J. Fluid Mech.* **21**, 1–20.

Lee, M. J., Kim, J. & Moin, P. 1990 Structure of turbulence at high shear rate. *J. Fluid Mech.* **216**, 561–583.

Lighthill, M. J. 1963 Introduction – boundary layer theory. *Laminar boundary layers*, ch. 2 (ed. L. Rosenhead). Clarendon.

Lighthill, M. J. 1968 Turbulence. *Proc. Osborne Reynolds Centenary Symposium, University of Manchester, Sept. 1968*. In *Osborne Reynolds and engineering science today* (ed. D. M. McDowell & J. D. Jackson). Manchester University Press 1970.

Lighthill, M. J. 1979 Waves and hydrodynamic loading. *Proc. BOSS '79, London*, 1–40.

Lyons, S. L., Hanratty, T. J. & McLaughlin, J. B. 1989 Turbulence-producing eddies in the viscous wall region. *AIChE Jl* **35**, 1962–1974.

Moffatt, H. K. 1967 The interaction of turbulence with strong wind shear. In *Atmospheric*

PHILOSOPHICAL TRANSACTIONS OF THE ROYAL SOCIETY A MATHEMATICAL, PHYSICAL & ENGINEERING SCIENCES

turbulence and radio waves propagation (ed. A. M. Yaglom & V. I. Tatarski), p. 139. Moscow: Nauka.

Moffatt, H. K. 1981 Some developments in the theory of turbulence. *J. Fluid Mech.* **106**, 27–47.

Moin, P. & Kim, J. 1982 Numerical investigation of turbulent channel flow. *J. Fluid Mech.* **118**, 341–377.

Moin, P. & Kim, J. 1985 The structure of the vorticity field in turbulent channel flow. 1. Analysis of instantaneous fields and statistical correlations. *J. Fluid Mech.* **155**, 441–464.

Muller, A. & Gyr, A. 1986 On the vortex formation in the mixing layer behind dunes. *J. hyd. Res.* **24**, 359–375.

Nakagawa, H. & Nezu, I. 1981 Structure of space-time correlations of bursting phenomena in an open-channel flow. *J. Fluid Mech.* **104**, 1–43.

Nezu, I. 1977 Turbulence intensities in open channel flows. *Proc. Japan Soc. Civil Engrs* **261**, 67–76.

Nikuradse, J. 1933 Stromungsgesetze in rauhen Rohren. *Forschg. Arb. Ing.-Wes.* no. 361.

Nychas, S. G., Hershey, H. C. & Brodkey, R. S. 1973 A visual study of turbulent shear flow. *J. Fluid Mech.* **61**, 513–540.

Paeschke, W. 1937 Experimentelle Untersuchungen zum Rauhigkeits- und Stabilitatsproblem in der bodennahen huftschicht. *Beitr. Phys. fr. Atmos.* **24**, 163–189.

Peridier, V. J., Smith, F. T. & Walker, J. D. A. 1991*a*, *b* Vortex induced boundary layer separation. Part I. The limit problem $Re \to \infty$; Part II. Unsteady interacting boundary layer theory. *J. Fluid Mech.* (In the press.)

Perry, A. E. & Joubert, P. N. 1963 Rough wall boundary layers in adverse pressure gradients. *J. Fluid Mech.* **17**, 193–211.

Perry, A. E., Schofield, W. H. & Joubert, P. N. 1969 Rough wall turbulent boundary layers. *J. Fluid Mech.* **37**, 383–413.

Perry, A. E., Lim, T. T. & Teh, E. W. 1981 A visual study of turbulent spots. *J. Fluid Mech.* **104**, 387–405.

Perry, A. E. & Chong, M. S. 1982 On the mechanism of wall turbulence. *J. Fluid Mech.* **119**, 173–217.

Perry, A. E., Henblest, S. & Chong, M. S. 1986 A theoretical and experimental study of wall turbulence. *J. Fluid Mech.* **165**, 163–199.

Perry, A. E., Lim, K. L. & Henblest, S. M. 1987 An experimental study of the turbulence structure in smooth- and rough-wall boundary layers. *J. Fluid Mech.* **177**, 437–466.

Piomelli, U., Ferziger, J. & Moin, P. 1989 New approximate boundary conditions for large eddy simulations in wall-bounded flows. *Phys. Fluids* A **1**, 1061–1068.

Praturi, A. K. & Brodkey, R. S. 1978 A stereoscopic visual study of coherent structures in turbulent shear flow. *J. Fluid Mech.* **89**, 251–272.

Raven, P. W. J. 1977 Turbulent boundary layer characteristics in open channel flow over fixed and mobile sand beds. Ph.D. dissertation, University of London.

Robinson, S. K. 1989 A review of vortex structures and associated coherent motions in turbulent boundary layers. *Second IUTAM Meeting on Structure of Turbulence and Drag Reduction*, Zurich, July.

Robinson, S. K., Kline, S. J. & Spalart, P. R. 1989 A review of quasi-coherent structures in a numerically simulated turbulent boundary layer. NASA Technical Memorandum 102191, May.

Rogers, M. M. & Moin, P. 1987 The structure of the vorticity field in homogeneous turbulent flows. *J. Fluid Mech.* **176**, 33–66.

Sene, K. J., Thomas, N. H. & Goldring, B. T. 1989 Planar plunge-zone flow patterns and entrained bubble transport. *J. hyd. Res.* **27**, 363–383.

Smith, C. R. & Metzler, S. P. 1983 The characteristics of low-speed streaks in the near-wall region of a turbulent boundary layer. *J. Fluid Mech.* **129**, 27–54.

Smith, C. R. & Schwartz, S. P. 1983 Observations of streamwise rotation in the near-wall region of a turbulent boundary layer. *Phys. Fluids* **26**, 641–652.

Smith, C. R. & Lu, L. J. 1988 The use of a template-matching technique to identify hairpin vortex

PHILOSOPHICAL TRANSACTIONS OF THE ROYAL SOCIETY A MATHEMATICAL, PHYSICAL & ENGINEERING SCIENCES

flow structures in turbulent boundary layers. *Near Wall Turbulence: 1988 Zaric Memorial Conf. Dubrovnik*. Hemisphere.

Smith, C. R., Walker, J. D. A., Haidari, A. H. & Taylor, B. K. 1989 Hairpin vortices in turbulent boundary layers: the implications for reduced surface drag. *Proc. 2nd IUTAM Symp. on Structure of Turbulence and Drag Reduction* (ed. A. Gyr). Springer-Verlag.

Smith, C. R. & Walker, J. D. A. 1990 A conceptual model of wall turbulence. *Boundary-layer structure workshop*. NASA Langley Research Centre, Hampton, Virginia, August 28–30.

Smith, F. T. 1991 Theoretical aspects of transition and turbulence in boundary layers. *29th AIAA Aerospace Sciences Meeting, Reno, Nevada, January*, Pap. no. AIAA 91-0331.

Smith, R. W. & Smits, A. J. 1991 Effect of Reynolds number on the large structure of turbulent boundary layers. *29th AIAA Aerospace Sciences Meeting, Reno, Nevada, January*, Pap. no. AIAA 91-0526.

Spalart, P. R. 1988 Direct simulation of a turbulent boundary layer up to $R = 1410$. *J. Fluid Mech.* **187**, 61–98.

Stuart, R. J. 1984 Three-dimensional characteristics of coherent flow structures in a turbulent boundary layer over a rough surface. Ph.D. dissertation, University of London.

Taylor, G. I. 1938 The spectrum of turbulence. *Proc. R. Soc. Lond.* A **164**, 476–490.

Theodorsen, T. 1952 Mechanism of turbulence. *2nd Midwestern Conf. on Fluid Mech., Ohio State University*, pp. 1–18.

Thomas, A. S. W. & Brown, G. L. 1977 Large structure in a turbulent boundary layer. *6th Australasian Hyd. and Fluid Mech. Conf., Adelaide, December*, pp. 407–410.

Townsend, A. A. 1961 Equilibrium layers and wall turbulence. *J. Fluid Mech.* **11**, 97–120.

Townsend, A. A. 1970 Entrainment and the structure of turbulent flow. *J. Fluid Mech.* **41**, 13–46.

Townsend, A. A. 1976 *The structure of turbulent shear flow*. Cambridge University Press.

Walker, J. D. A. 1990 Models based on dynamical features of the wall layer. *Appl. Mech Rev.* **43**, S232–S239.

Walker, J. D. A. & Herzog, S. 1988 Eruption mechanisms for turbulent flows near walls. *2nd Int. Symp. on Transport phenomena in turbulent flows* (ed. M. Hirata & V. Kasagi), 145–156. New York: Hemisphere.

Walker, J. D. A., Abbott, D. E., Schnarnhorst, R. K. & Weigand, G. G. 1989 Wall-layer model for the velocity profile in turbulent flows. *AIAA J.* **27**, 140–149.

Wallace, J. M. 1985 *The vortical structure of bounded turbulent shear flow. Lecture Notes in Physics 235*, pp. 253–268. Springer-Verlag.

Williams, D. R., Fasel, H. & Hama, F. R. 1984 Experimental determination of the three-dimensional vorticity field in the boundary-layer transition process. *J. Fluid Mech.* **149**, 179–203.

Yaglom, A. M. 1979 Simlarity laws for constant-pressure and pressure-gradient turbulent wall flows. *A. Rev. Fluid Mech.* **11**, 505–540.

PHILOSOPHICAL TRANSACTIONS OF THE ROYAL SOCIETY A MATHEMATICAL, PHYSICAL & ENGINEERING SCIENCES

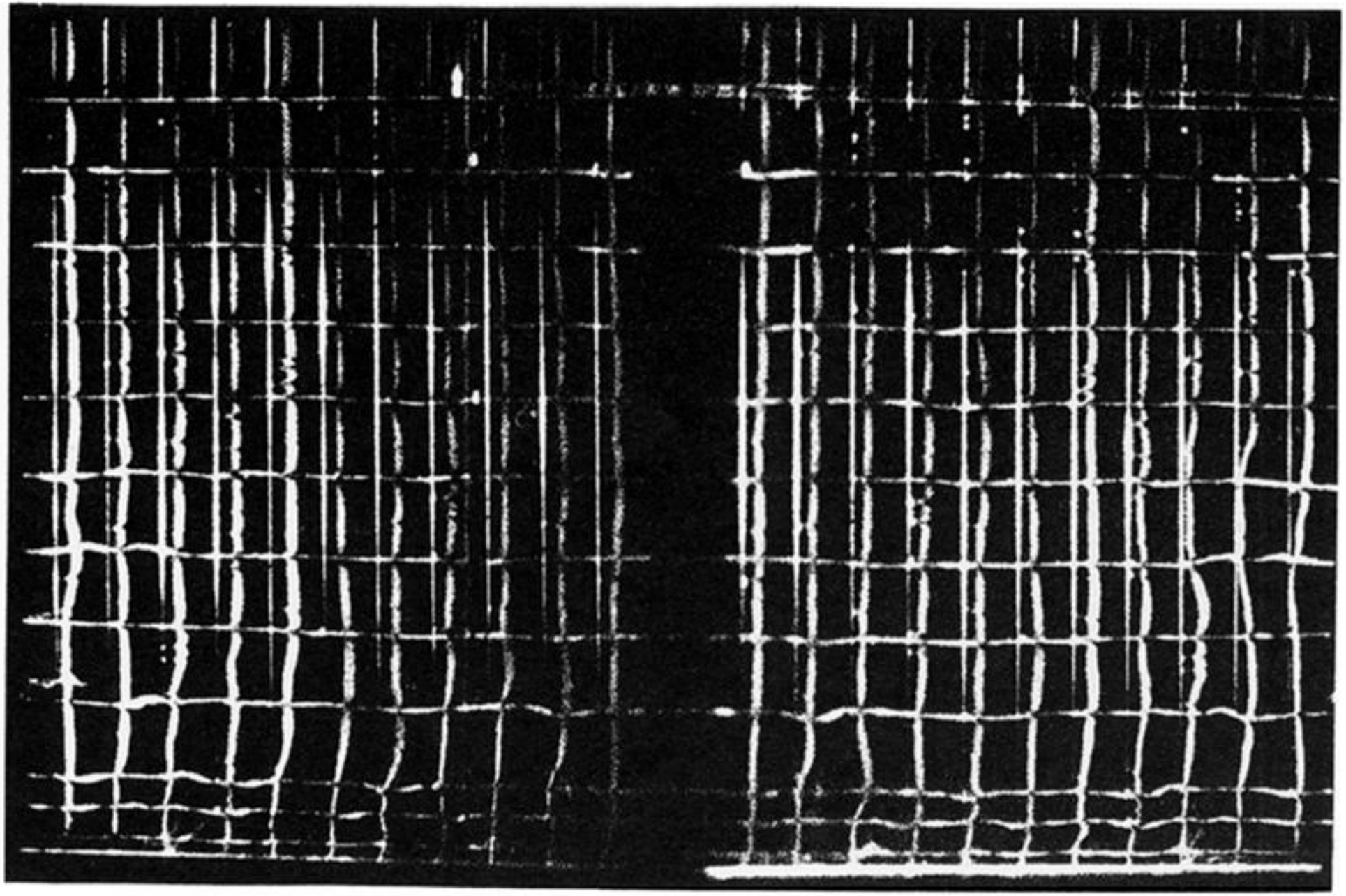

gure 4. Typical film frame showing stereoscopic images of the hydrogen bubble tracer grids.

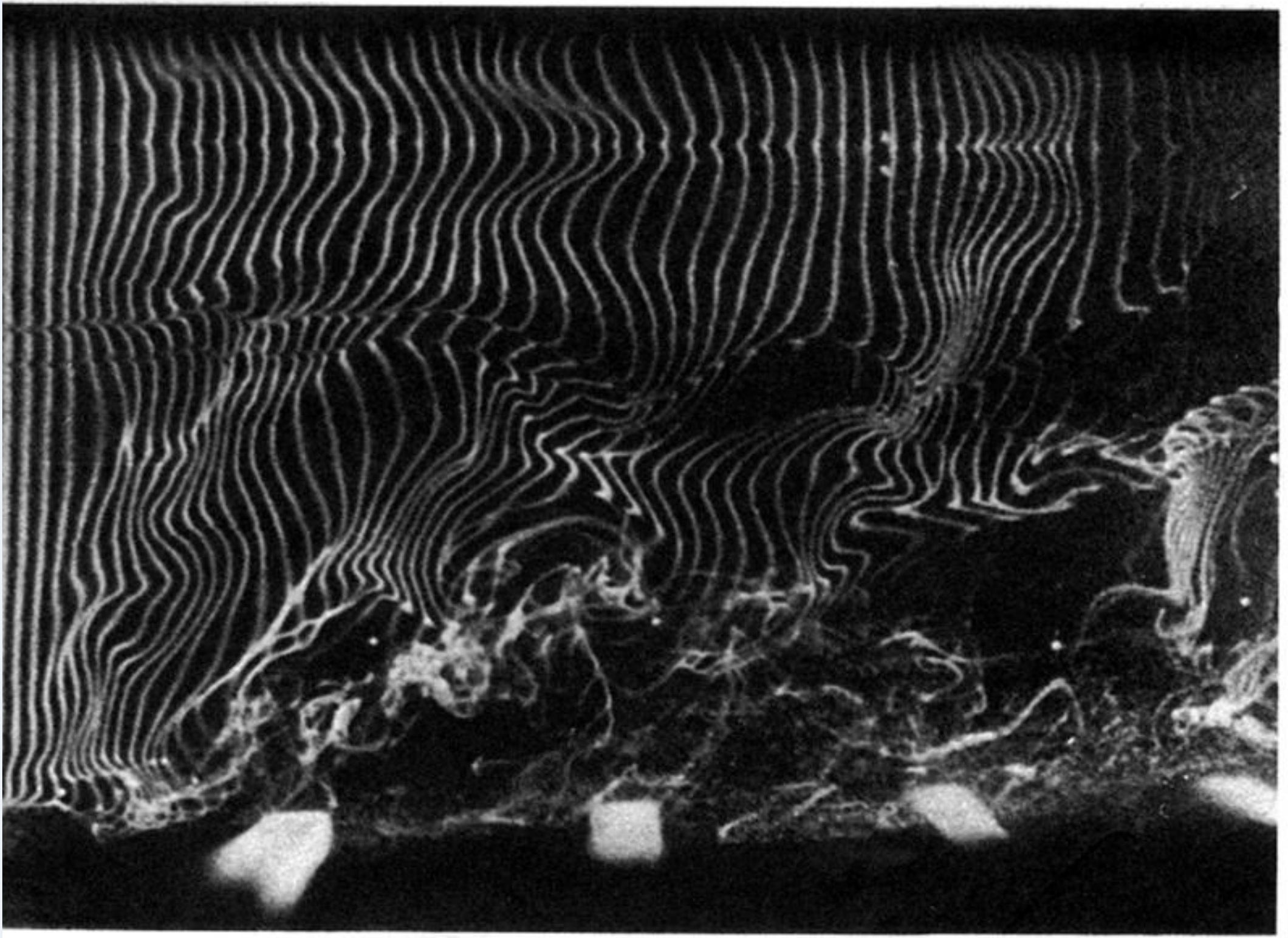

Figure 7. Hydrogen bubble visualization of general flow structure.

PHILOSOPHICAL TRANSACTIONS OF THE ROYAL SOCIETY A MATHEMATICAL, PHYSICAL & ENGINEERING SCIENCES

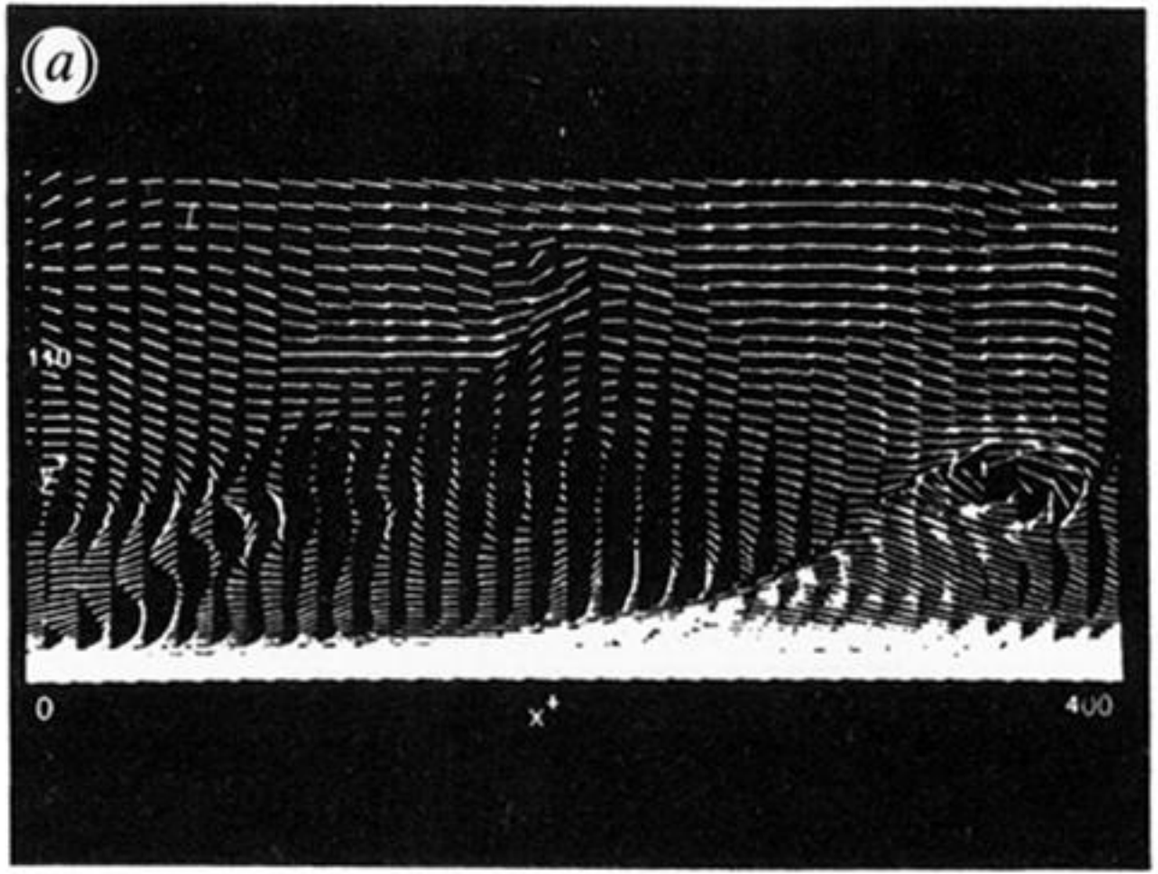

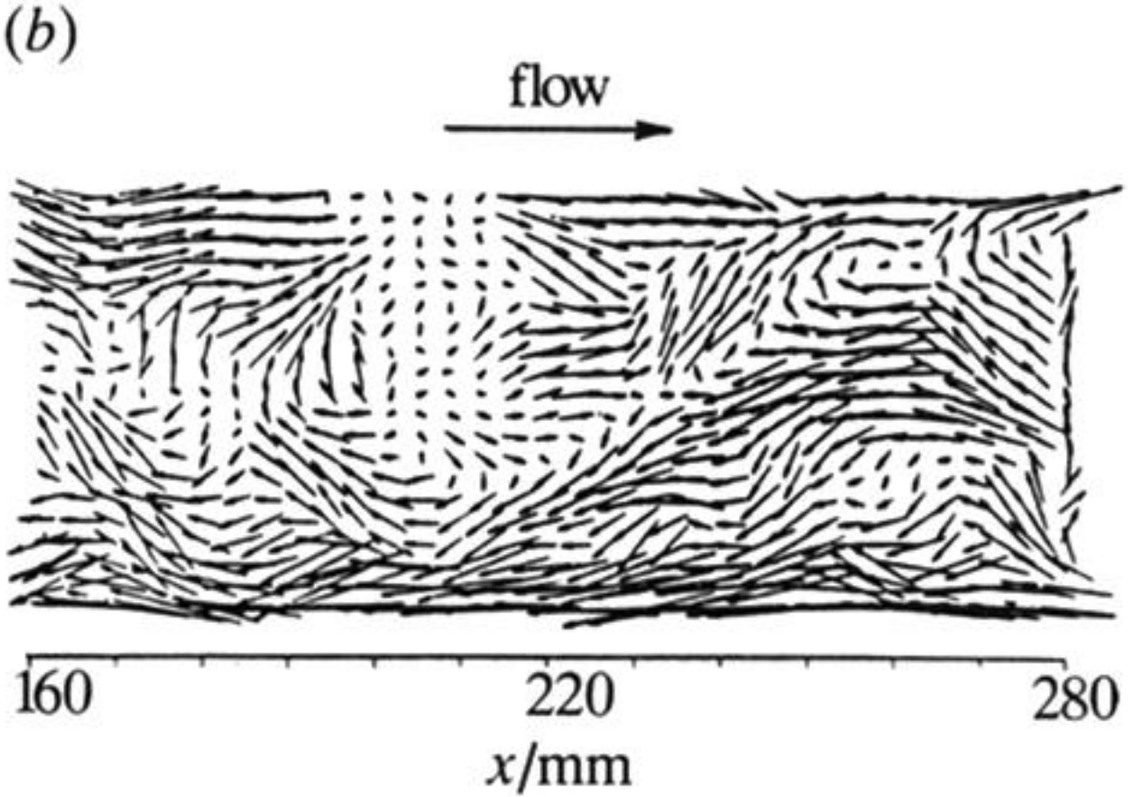

gure 9. Examples of shear layer roll-up with section through transverse 'head' vortex.) Numerical stimulation of smooth wall boundary layer (Robinson *et al.* 1989). (*b*) Present rough all study (segment 1, figure 8).

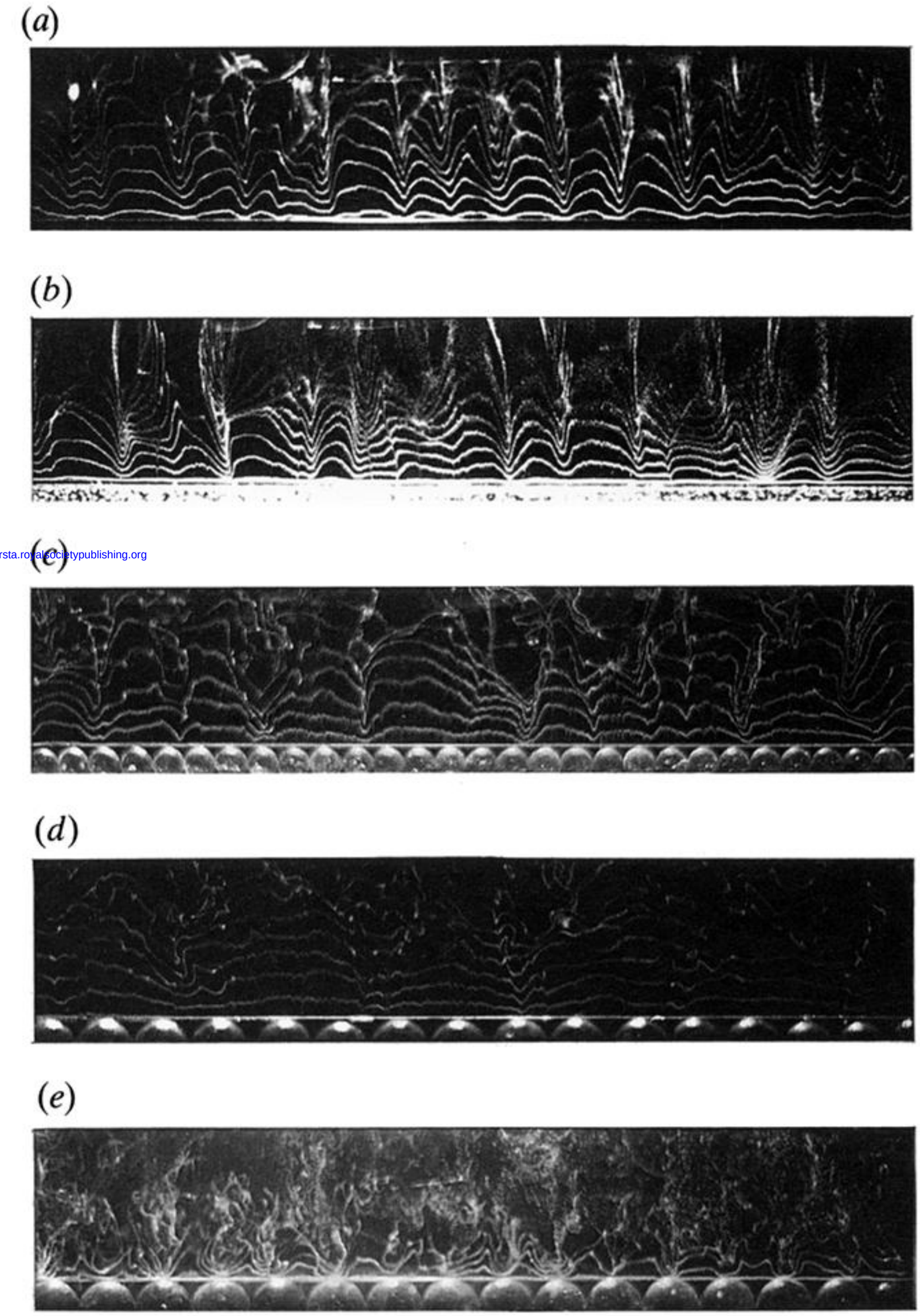

igure 17. Near wall flow structure visualized by hydrogen bubble tracers generated on transverse ire parallel to the bed. Bed roughness conditions and wire distance from top of roughness, y_1, follows: (*a*) smooth: $y_1 = 1$ mm; (*b*) $k = 1.15$ mm, $y_1 = 1$ mm; (*c*) $k = 6$ mm, $y_1 = 3$ mm;) $k = 12$ mm, $y_1 = 3.5$ mm; (*e*) $k = 12$ mm, $y_1 = 0.55$ mm.